iScience

CellPress
OPEN ACCESS

Article

Partial Replacement of Nucleosomal DNA with Human FACT Induces Dynamic Exposure and Acetylation of Histone H3 N-Terminal Tails

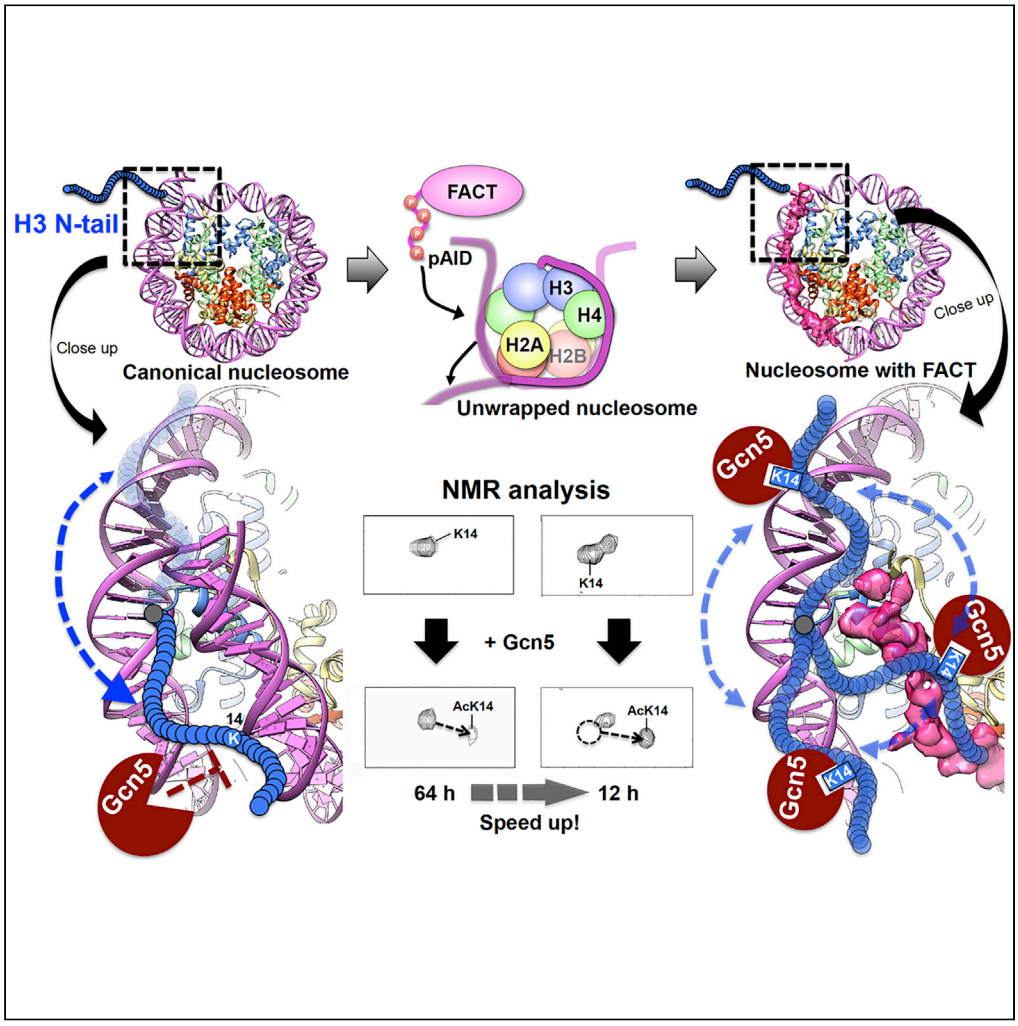

Yasuo Tsunaka, Hideaki Ohtomo, Kosuke Morikawa, Yoshifumi Nishimura

nisimura@yokohama-cu.ac.jp

HIGHLIGHTS

H3 N-tail, restricted to two DNA gyres of nucleosome, is protected from Gcn5

H3 N-tail is dynamically exposed by replacement of nucleosomal DNA with pAID of FACT

Gcn5 efficiently acetylates accessible H3 N-tail of nucleosome with FACT

FACT acts as a modulator for dynamic behavior of H3 tails in nucleosome

Tsunaka et al., iScience *23*, 101641
October 23, 2020
https://doi.org/10.1016/j.isci.2020.101641

iScience

CellPress
OPEN ACCESS

Article

Partial Replacement of Nucleosomal DNA with Human FACT Induces Dynamic Exposure and Acetylation of Histone H3 N-Terminal Tails

Yasuo Tsunaka,[1] Hideaki Ohtomo,[1] Kosuke Morikawa,[2] and Yoshifumi Nishimura[1,3,4,*]

SUMMARY

The FACT (facilitates chromatin transcription) complex, comprising SPT16 and SSRP1, conducts structural alterations during nucleosome unwrapping. Our previous cryoelectron microscopic (cryo-EM) analysis revealed the first intermediate structure of an unwrapped nucleosome with human FACT, in which 112-bp DNA and the phosphorylated intrinsically disordered (pAID) segment of SPT16 jointly wrapped around the histone core instead of 145-bp DNA. Using NMR, here we clarified that the histone H3 N-terminal tails, unobserved in the cryo-EM structure, adopt two different conformations reflecting their asymmetric locations at entry/exit sites: one corresponds to the original nucleosome site buried in two DNA gyres (DNA side), whereas the other, comprising pAID and DNA, is more exposed to the solvent (pAID side). NMR real-time monitoring showed that H3 acetylation is faster on the pAID side than on the DNA side. Our findings highlight that accessible conformations of H3 tails are created by the replacement of nucleosomal DNA with pAID.

INTRODUCTION

In eukaryotic cells, the functional structures of chromatin are orchestrated in a hierarchical manner. The dynamic conversion of these hierarchical structures is involved in regulating DNA accessibility to protein complexes or RNA molecules and thus directs the dynamic modulation of gene expression in nuclear events: DNA replication, repair, transcription, and so on (Brahma and Henikoff, 2020; Klemm et al., 2019; Lai and Pugh, 2017; Stewart-Morgan et al., 2020). The fundamental repeating unit of chromatin is nucleosome, in which 145–147 bp of DNA wraps around an octamer containing two copies each of histones H2A, H2B, H3, and H4 (Luger et al., 1997). The N-terminal tails (N-tails) of all histones and the C terminus of H2A stick out from the nucleosome core particle. All the histone tails extensively undergo post-translational modifications (PTMs), which are essential for epigenetic cell memory (Stewart-Morgan et al., 2020; Suganuma and Workman, 2011; Zentner and Henikoff, 2013). The modified tails interact with other proteins through functional domains, such as bromodomains, chromodomains, and plant homeodomain (PHD) fingers, to recruit multiple protein complexes to nucleosome (Andrews et al., 2016; Musselman et al., 2012). The histone tails can also interact with DNA to alter nucleosomal stability (Iwasaki et al., 2013), the rate of DNA unwrapping (Andresen et al., 2013), and protein accessibility to nucleosome (Morrison et al., 2018). Owing to their conformational flexibility, however, the histone tails are mostly invisible in crystal and electron microscopic (EM) structures of nucleosome complexes (Farnung et al., 2017; He et al., 2020; Kato et al., 2017; Kujirai et al., 2018; Liu et al., 2020; Luger et al., 1997; Mayanagi et al., 2019; Tachiwana et al., 2011; Tsunaka et al., 2005; Vasudevan et al., 2010). On the other hand, nuclear magnetic resonance (NMR) spectroscopy has revealed that histone tails have a high degree of structural flexibility and higher solvent accessibility relative to the globular domain (Morrison et al., 2018; Stützer et al., 2016; Zhou et al., 2012).

An essential histone chaperone, FACT (facilitates chromatin transcription), accomplishes both assembly and disassembly of nucleosomes during transcriptional elongation (Belotserkovskaya et al., 2003; Ramachandran et al., 2017) and at the boundary between heterochromatin and euchromatin (Nakayama et al., 2007, 2012). During the initial step of disassembly, FACT interacts with the exposed DNA-binding surface of histones within nucleosome unwrapped by other factors (McCullough et al., 2018; Ramachandran et al., 2017; Safina et al., 2017; Tsunaka et al., 2016; Valieva et al., 2017). In particular, we previously showed that the extensively phosphorylated C-terminal acidic intrinsically disordered (pAID) segment of SPT16 within human FACT (hFACT),

[1]Graduate School of Medical Life Science, Yokohama City University, 1-7-29 Suehiro-cho, Tsurumi-ku, Yokohama 230-0045, Japan

[2]Department of Gene Mechanisms, Graduate School of Biostudies, Kyoto University, Yoshida-konoemachi, Sakyo-ku, Kyoto 606-8501, Japan

[3]Graduate School of Integrated Sciences for Life, Hiroshima University, 1-4-4 Kagamiyama, Higashi-Hiroshima 739-8528, Japan

[4]Lead Contact

*Correspondence: nisimura@yokohama-cu.ac.jp

https://doi.org/10.1016/j.isci.2020.101641

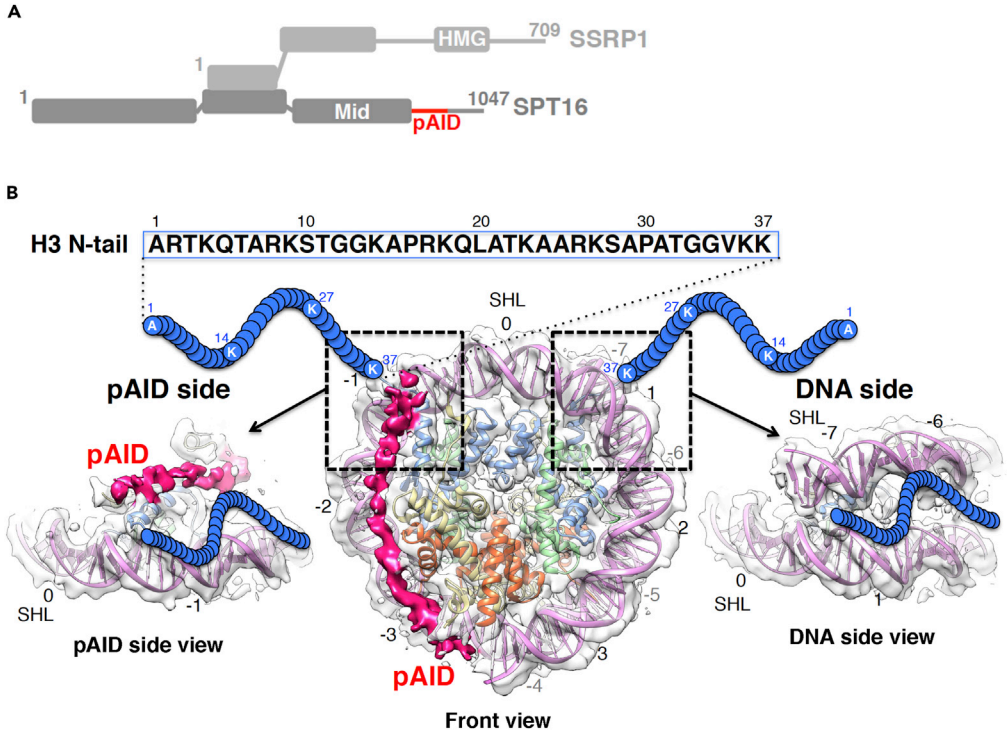

Figure 1. Structural Location of the Two H3 N-Tails in the 112-bp DNA/pAID Nucleosome

(A) Domain organization of human FACT. Full-length FACT and pAID (red) proteins were used in this study.

(B) Cryo-EM structure of the 112-bp DNA/pAID nucleosome. Three views of the EM density map (EMD-9639) are superimposed on the nucleosome structure (PDB: 2CV5) lacking the 33-bp DNA. Visualization of the EM maps and fitting of nucleosome structures into the maps were performed using UCSF Chimera (Pettersen et al., 2004). pAID is shown in a deep pink density. H2A, H2B, H3, H4, and DNA are colored yellow, red, blue, green, and orchid, respectively. Blue circular chains denote the H3 N-tails, which were unobserved in the EM structure. The sequence of the H3 N-tail is shown above. Superhelix locations (SHL), which represent the number of double turns from the dyad axis of the canonical nucleosome (0), are indicated.

comprising the SPT16 and SSRP1 subunits (Figure 1A), initially binds to the H2B N-tail that is detached from nucleosomal DNA by a double-strand break (Tsunaka et al., 2016), and the pAID-deleted mutant of hFACT shows a significantly reduced interaction with the unwrapped nucleosome (Mayanagi et al., 2019). Thus, pAID within hFACT is thought to bind to the unwrapped nucleosome in the initial step of disassembly. In addition, our previous study clarified for the first time such transient intermediate structures in nucleosome unwrapping mediated by hFACT (Figure 1B) (Mayanagi et al., 2019). The 112-bp nucleosome, which is wrapped by a shorter DNA rather than the canonical nucleosome DNA (145–147 bp), was used as a model for the transient intermediate. The resulting cryo-EM structure revealed that the pAID segment of SPT16 (Figure 1A) asymmetrically wraps around the exposed DNA-binding surface of H3, H2A, and H2B in the 112-bp nucleosome (Figure 1B). Thus, hFACT can completely retain the nucleosome core structure by partially replacing approximately 33–43 bp of nucleosomal DNA of the conventional nucleosome with pAID. In the cryo-EM structure, however, the histone tails were not visualized (Figure 1B) (Mayanagi et al., 2019), similar to the structures of most nucleosomal complexes (Armache et al., 2019; Ehara et al., 2019; Farnung et al., 2017; He et al., 2020; Kato et al., 2017; Kujirai et al., 2018; Liu et al., 2020; Luger et al., 1997; Tachiwana et al., 2011; Tsunaka et al., 2005; Vasudevan et al., 2010). Therefore, the dynamic structures of histone tails remain elusive in the unwrapped nucleosome structure, which is putatively formed before chromatin remodeling.

Here, we have used NMR spectroscopy to examine the dynamic structures of histone tails in the 112-bp nucleosome complexed with pAID of human SPT16 (112-bp DNA/pAID nucleosome), in particular focusing on the two H3 N-tails that are symmetrically located at the entry/exit sites of nucleosomal DNA in the conventional nucleosome, but in asymmetric environments in the cryo-EM structure (Figure 1B). Among the histone tails, the H3 N-tails are relatively distinct because they comprise a most extensively disordered

region and undergo more than 30 post-translational modification (PMTs) related to interactions with several effector domains (Bannister and Kouzarides, 2011; Chi et al., 2010). Intriguingly, most residues of the H3 N-tails in the 112-bp DNA/pAID nucleosome showed two separate NMR signals, corresponding to the asymmetric locations of the two H3 N-tails: one lies in an environment similar to that of the conventional H3 N-tail location (Figure 1B, DNA side view), whereas the other, sandwiched between pAID and DNA, is more exposed to solvent (Figure 1B, pAID side view). Our enzymatic analyses using Gcn5 showed that the pAID side tail is acetylated much faster relative to the DNA side tail or the N-tails in the canonical nucleosome. Taken together, these findings imply that such changes in the dynamic behavior of the histone tails may play key roles in switching between heterochromatin and euchromatin.

RESULTS

Distinct Chemical Environments around the Two H3 N-Tails in the 112-bp DNA/pAID Nucleosome

To investigate the behavior of histone H3 N-tails in the unwrapped nucleosome, we reconstituted the 112-bp DNA/pAID nucleosome with $^{2}H/^{15}N$ or $^{2}H/^{15}N/^{13}C$ -labeled human H3 and unlabeled human H2A, H2B, H4, 112-bp 601 DNA, and the pAID protein comprising the SPT16 residues Glu926–Glu964 of hFACT (Figures 1A and 1B). In previous 2D ^{1}H-^{15}N hetero-nuclear single quantum coherence (HSQC) spectra of nucleosomes in solution, NMR signals from residues within the structural core are unobservable, whereas those of the flexible histone tails are clearly observed (Morrison et al., 2018; Stützer et al., 2016; Zhou et al., 2012). Consistent with those studies, the signal assignments of the 112-bp DNA/pAID nucleosome confirmed that, except for Pro16 and Pro30, the observed peaks derived from residues Arg2–Lys37 in the histone H3 N-tails (Figure 2A). Notably, we observed two separate signals for Arg2–Lys9, Gly12, Lys14, Ala15, Arg17–Ala29, and Ala31–Lys36 (Figure 2A), reflecting asymmetric environments around the two H3 N-tails in the complex (Figure 1B). Under the same conditions, the NMR spectrum of the 145-bp nucleosome including $^{2}H/^{15}N$-labeled H3 showed one signal for the residues in the H3 N-tails, except for Arg2, Gln5, Gln19, and Thr32–Val35, which all showed a major signal together with a minor signal (Figure 2B). This indicates that environments around the two H3 N-tails in the canonical nucleosome are almost symmetric, in agreement with previous studies (Morrison et al., 2018; Stützer et al., 2016; Zhou et al., 2012). More importantly, the signals in the 145-bp nucleosome corresponded approximately to one of the two separate signals in the 112-bp DNA/pAID nucleosome (Figure 2B), indicating that one of the H3 N-tails in the 112-bp DNA/pAID nucleosome apparently adopt a conformation similar to those in the 145-bp nucleosome.

Our previous study showed that the addition of extra DNA dissociated pAID from the 112-bp DNA/pAID nucleosome, with the subsequent replacement of pAID by the extra DNA (Mayanagi et al., 2019). To determine whether the addition of extra DNA would affect the two separate signals of the H3 N-tails in 112-bp DNA/pAID nucleosome, we titrated 33-bp DNA into the H3-labeled nucleosome. One of two signals almost disappeared or was impaired upon the addition of DNA up to a two-fold excess over the 112-bp DNA/pAID nucleosome (Figure S1A), whereas the remaining signals were roughly equivalent to those in the 145-bp nucleosome (Figure S1B). These results indicate that the asymmetric environments of the two H3 N-tails converge into a symmetric environment similar to that in the canonical nucleosome on the addition of extra DNA. Thus, in the NMR spectrum of the 112-bp DNA/pAID nucleosome, the signals corresponding to the canonical nucleosome are ascribed to the H3 N-tail on the DNA side, and the other signals are assigned to the H3 N-tail on the pAID side (Figures 1B, 2B, 3A, and 3B).

To further probe the environment around the H3 N-tail on the pAID side in the 112-bp DNA/pAID nucleosome, we measured the chemical shift perturbations upon titration of NaCl into the 145-bp nucleosome, which should induce dissociation of the H3 N-tails from DNA. As expected, the signals for Thr3–Arg8, Gly12, Lys14, Ala15, Arg17–Gln19, Ala21, Lys23–Ala29, Thr32–Gly34, and Lys36 were shifted on NaCl titration (Figure S2A). In particular, the signals observed at 200 mM NaCl were almost equivalent to the pAID side signals in the 112-bp DNA/pAID nucleosome (Figures 3A, 3B, and S2B). This indicates that the pAID side H3 N-tail is relatively exposed to the solvent, similar to the H3 N-tails in the canonical nucleosome at 200 mM NaCl; such a high salt concentration should weaken the electrostatic interaction between DNA and H3 N-tails.

Significant chemical shift changes between the pAID and DNA side N-tails were observed in two basic segments: basic 1 (B1), consisting of Lys4–Lys9, and basic 2 (B2), comprising Arg17–Ser28 (Figure 4A). These basic segments are connected thorough a linker 1 (L1), composed of Ser10–Ala15, and the B2 segment is connected to the nucleosome core by another linker (L2), comprising Ala31–Lys36; both L1 and L2

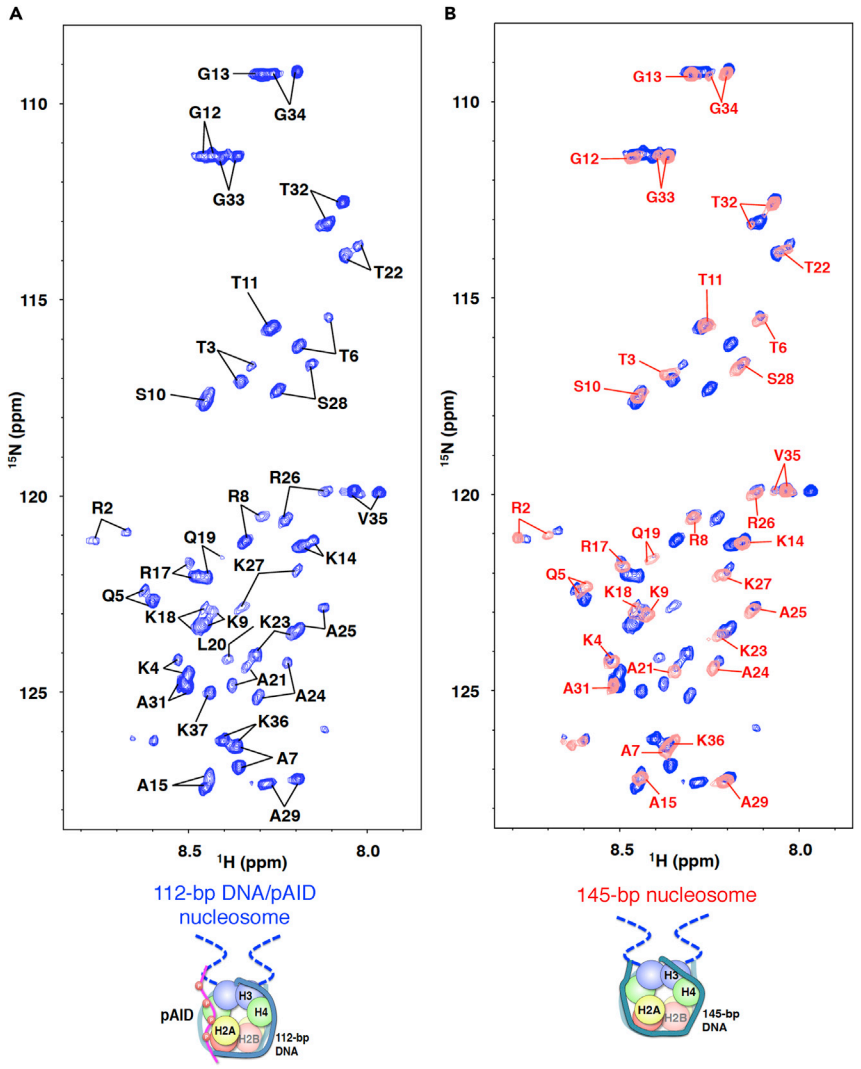

Figure 2. Two Separate NMR Signals from H3 N-Tails in the 112-bp DNA/pAID Nucleosome

(A) Backbone resonance assignments of the 112-bp DNA/pAID nucleosome in the 2D ^{1}H-^{15}N HSQC spectrum. Cartoon model of the nucleosomal complex is shown below. The histone proteins and DNA are colored as follows: H2B (red), H2A (yellow), H3 (blue), H4 (green), and DNA (light sea green). The H3 N-tails are indicated by dotted strings. pAID is colored magenta. Red open circles labeled with P indicate phosphorylation.

(B) Spectral comparison of 2D ^{1}H-^{15}N HSQC spectra between the 145-bp nucleosome (red) and the 112-bp DNA/pAID nucleosome (blue). Signal assignments in the 145-bp nucleosome are labeled. Cartoon model of the nucleosomal complex is below.

See also Figure S1.

showed smaller chemical shift changes (Figure 4A). Overall, the chemical shift changes of the H3 N-tail in the 112-bp DNA/pAID nucleosome showed a similar pattern to those in the 145-bp nucleosome between 0 and 200 mM NaCl conditions (Figure 4B). They were also similar to chemical shift changes previously observed between free H3 peptide comprising the H3 N-terminal residues and H3 N-tails in either the 147-bp nucleosome (Morrison et al., 2018) or the 187-bp nucleosome containing linker DNA (Stützer et al., 2016). Notably, the B1 and B2 segments in the H3 N-tails equally showed larger chemical shift changes for interaction with nucleosomal DNA in different nucleosomes, independent of the DNA length and buffer conditions (Figures 4A and 4B) (Morrison et al., 2018; Stützer et al., 2016).

The ^{15}N{^{1}H} heteronuclear nuclear Overhauser effect (NOE) measurements for the 112-bp DNA/pAID nucleosome revealed no secondary structure in the H3 N-tails on either the DNA or the pAID side, similar

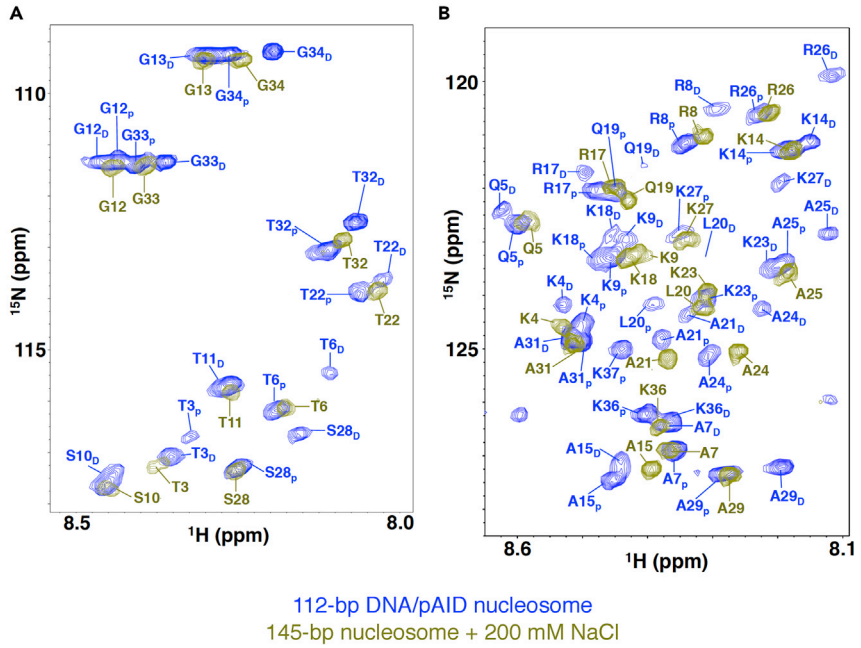

Figure 3. The Two H3 Tails Adopt Distinct Conformations in the 112-bp DNA/pAID Nucleosome

Two expanded regions of the spectrum of Figure 1B are separately shown (A and B). Spectral comparison of 2D ^{1}H-^{15}N HSQC spectra between the 145-bp nucleosome at 200 mM NaCl (yellow) and the 112-bp DNA/pAID nucleosome (blue). As described in the text, the two separate signals from each H3 N-tail residue in the 112-bp DNA/pAID nucleosome are assigned to H3 N-tails on the pAID side (labeled by subscript p) and the DNA side (labeled by subscript D).
See also Figure S2.

to measurements for the 145-bp nucleosome (Figures 4C and 4D). The NOE values of the pAID side signals for Lys4–Thr6, Arg8, Lys9, Ala15, Arg17, Ala21–Ala29, and Lys36 all showed a small decrease, relative to the values of the corresponding residues on the DNA side (Figure 4C). Overall, the DNA side signals for Lys4–Thr6, Arg8, Ala15, Arg17–Gln19, Ala21–Ala24, Arg26–Ala29, Ala31, Thr32, Gly34, and Val35 showed NOE values similar to those of the corresponding residues in the 145-bp nucleosome (Figures 4C and 4D). These results suggest that, when compared with the pAID side H3 N-tail, the H3 N-tails on the DNA side and in the canonical nucleosome are more restricted in terms of their mobility. For Thr3 and Val35, the NOE values of the pAID side signals were higher than those of the DNA side signals (Figure 4C). The pAID side signals for Thr3 and Val35 also differed in chemical shift from the corresponding signals in the 145-bp nucleosome at 200 mM NaCl (Figures 3A and S2C). Thr3 and Val35 on the pAID side seem to reflect a binding state with an unknown moiety, such as the histone surface exposed by the replacement of DNA with pAID.

Even in the 145-bp nucleosome, we observed two different NMR signals for Arg2, Gln5, Gln19, and Thr32–Val35 (Figure 2B), suggesting that these residues adopt two different conformations for the same H3 N-tail. For residues Gln5, Gln19, and Val35, the chemical shift difference between the two signals was very small when compared with that for the corresponding residues in the 112-bp DNA/pAID nucleosome (Figures 2B and S2C), suggesting that these residues adopt two similar DNA-contact conformations in the 145-bp nucleosome. Comparison of the signal intensities and chemical shifts between the two signals for residues Thr32–Gly34 suggested that these two signals correspond to a major DNA contact and a minor exposed conformation for the same H3 N-tail (Figure 2B). In the 112-bp DNA/pAID nucleosome (Figure 2A), by contrast, the two signals for residues Thr32–Gly34 showed similar strong intensities, suggesting that both conformations are major and likely to correspond to the H3 N-tails of the respective DNA and pAID sides. Exceptionally, Arg2 may adopt two different conformations for the same tail regardless of the DNA and pAID sides even in the 112-bp DNA/pAID nucleosome, because it exhibited two separate and equivalent signals similar to those observed after the addition of 33-bp DNA, as well as those in the 145-bp nucleosome (Figures 2B, S1B, and S2D). It is likely that the two conformations of Arg2 may be due to the fluctuating N terminus.

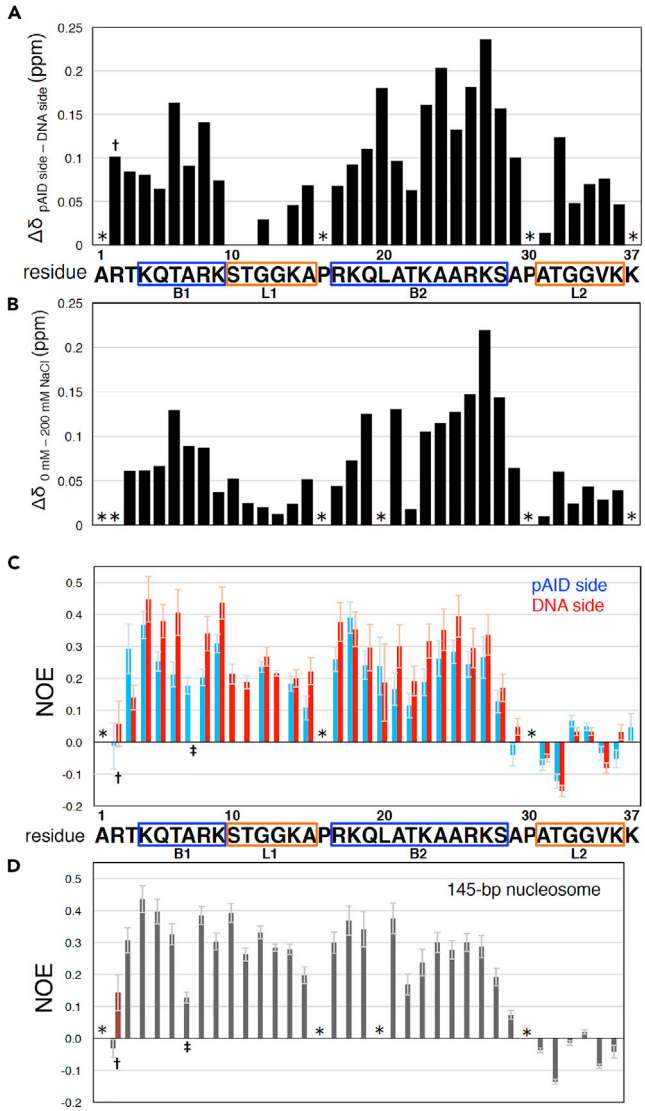

Figure 4. Chemical Shift Differences and Heteronuclear NOE Values of the H3 N-Tails in the Nucleosomal Complexes

(A and B) Histograms showing H3 N-tail chemical shift differences between the pAID and DNA sides in the 112-bp DNA/pAID nucleosome (A) and between 0 and 200 mM NaCl conditions for the 145-bp nucleosome (B). Chemical shift differences are plotted against the residue number of the H3 N-tails. Asterisks (*) indicate residues that were either not observed or not assigned. The dagger (†) indicates Arg2, for which the chemical shift difference was calculated for two separate signals that were not correctly assigned to either the pAID or DNA side H3 N-tails.

(C and D) Profiles of the $^{15}N\{^{1}H\}$ heteronuclear NOE values of H3 N-tails in the 112-bp DNA/pAID nucleosome (C) and the 145-bp nucleosome (D). NOE values are plotted against the residue numbers of the H3 N-tails. Asterisks (*) indicate residues that were either not observed or not assigned. The pAID and DNA side signals in the 112-bp DNA/pAID nucleosome are shown in blue and red, respectively. The dagger (†) indicates Arg2, for which the value of the right signal (R2 in Figure S2D) is nominally shown in red and the value of the left signal (R2* in Figure S2D) is shown in blue (112-bp DNA/pAID nucleosome) or gray (145-bp nucleosome). The double dagger (‡) indicates Arg7, for which the signals on the DNA side and in the 145-bp nucleosome were not correctly calculated owing to severe overlap with Lys36 signals, as shown in Figures 2A and 2B. Error bars were calculated on the basis of the signal to noise ratio.

The 112-bp DNA/FACT Nucleosome Is Highly Susceptible to H3 Acetylation

In the 112-bp DNA/pAID nucleosome, the more exposed H3 N-tail on the pAID side is expected to show greater accessibility to histone modification enzymes. Therefore, to compare the reaction of the 112-bp

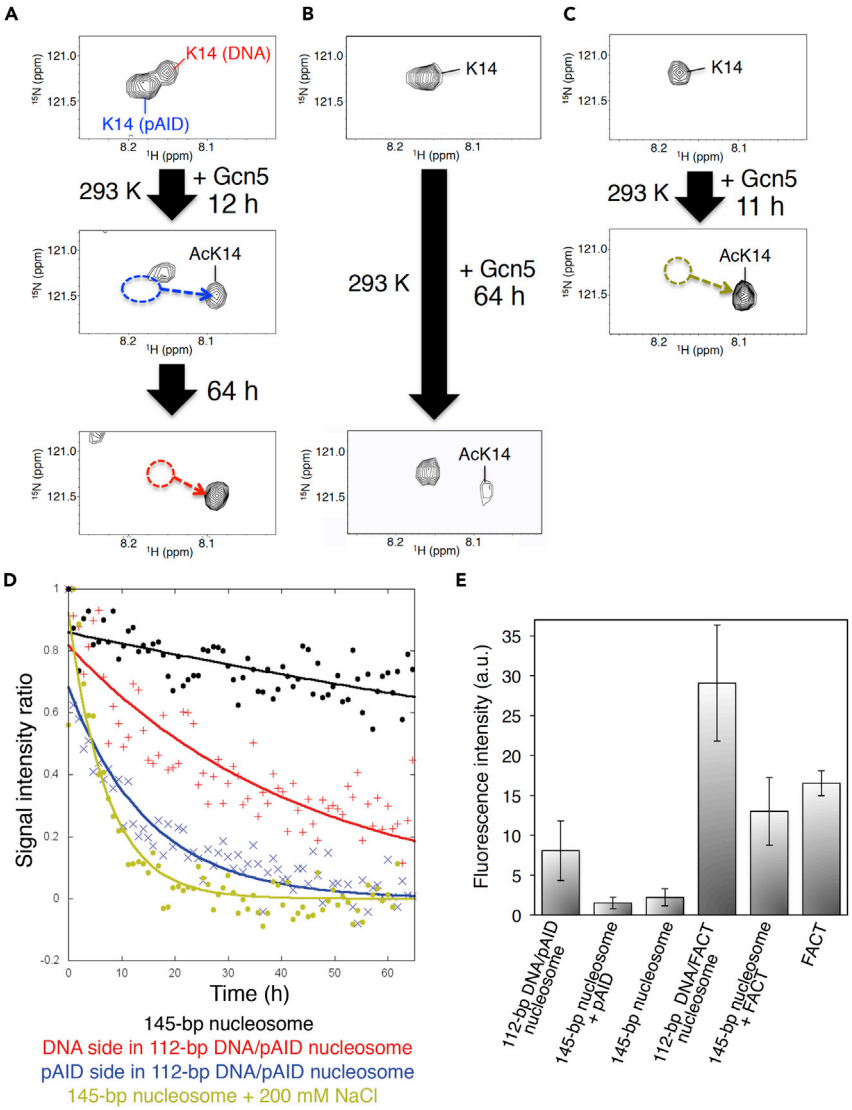

Figure 5. Comparison of H3 K14 Acetylation between the Canonical Nucleosome and Nucleosomal Complexes with hFACT Proteins

(A–C) Expanded view of the ^{1}H-^{15}N NMR spectrum at Lys14 of the H3 N-tail in the 112-bp DNA/pAID nucleosome (A), the 145-bp nucleosome (B), and the 145-bp nucleosome at 200 mM NaCl (C) during acetylation by Gcn5.

(D) Time-resolved NMR profiling of consecutive enzymatic reactions. Red, blue, black, and yellow plots show the raw values of the signal intensity ratio at Lys14 on the DNA and pAID sides in the 112-bp DNA/pAID nucleosome and in the 145-bp nucleosome at 0 and 200 mM NaCl, respectively. Values were calculated by setting the signal intensity before the reaction or after 1 h (200 mM NaCl) as 1. The decay curves were fitted with first-order equations using Gnuplot.

(E) Fluorescence HAT assays of the indicated nucleosomal complexes with hFACT proteins. HAT activity was quantified by the fluorescence intensity measured after the reaction. Averages from at least three independent experiments are shown; error bars represent SD. Addition of hFACT causes unexpected background, probably because Gcn5 may partly acetylate lysine residues within hFACT.

See also Figure S3.

DNA/pAID and 145-bp nucleosomes incorporating ^{2}H/^{15}N-labeled H3 with the catalytic domain of the human histone acetyltransferase (HAT) Gcn5, we recorded the ^{1}H-^{15}N HSQC spectra every hour at 293 K (Figures 5A–5D and S3A). Gcn5 is known to acetylate Lys14, the main target site on H3 (Figure 1B). After 12 h, the pAID side signal for Lys14 was almost completely converted to the acetylated signal (Figure 5A). By contrast, the signal intensity on the DNA side was more slowly reduced when compared with the pAID

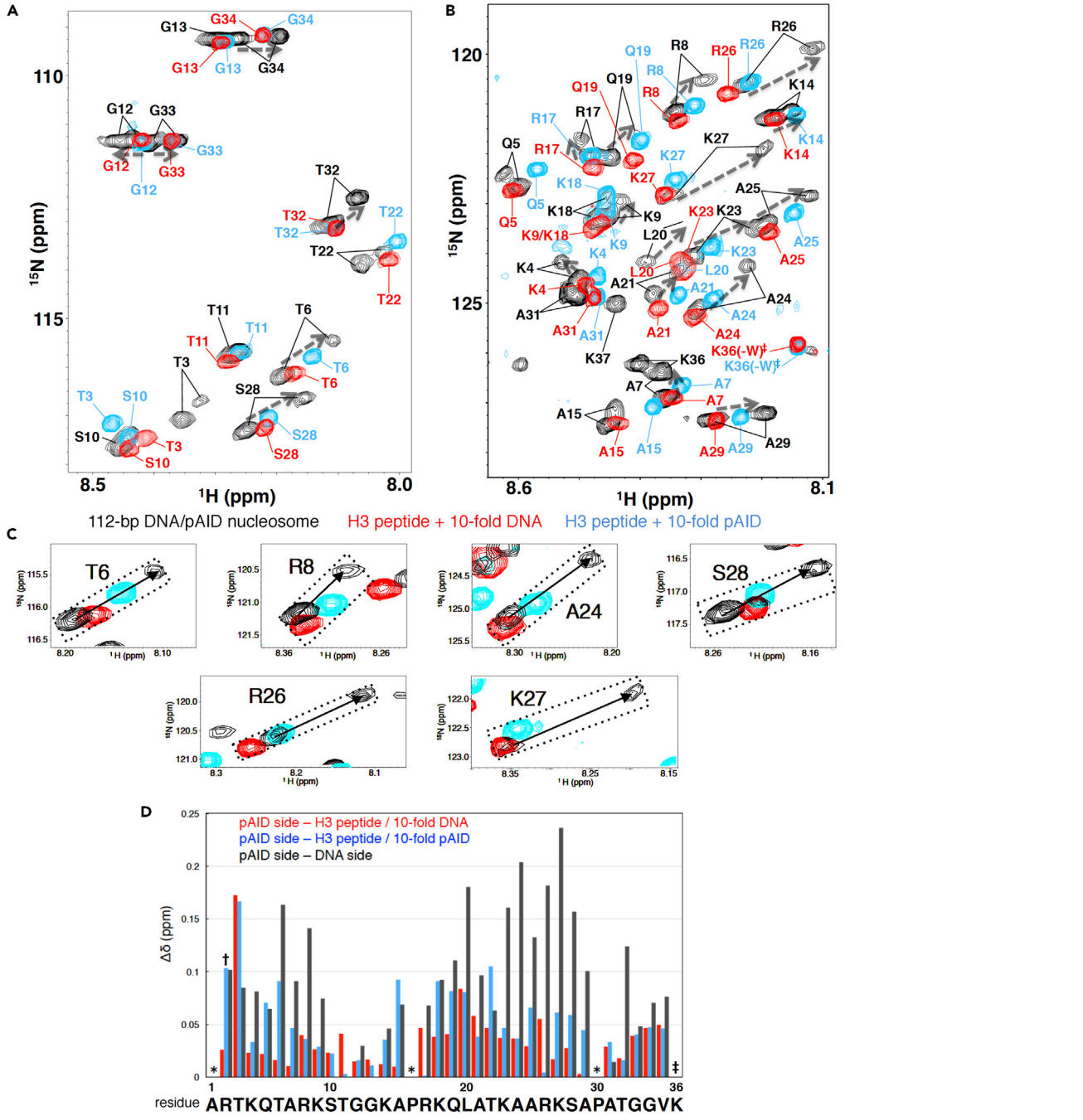

Figure 6. Conformational Comparison between the pAID- or DNA-Bound H3 Peptide and the Two H3 N-Tails in the 112-bp DNA/pAID Nucleosome

Two spectral regions are separately shown (A and B). Spectral comparison of 2D ^{1}H-^{15}N HSQC spectra between the H3 peptide upon the 10-fold addition of DNA (red) or pAID (cyan) and the 112-bp DNA/pAID nucleosome (black). Arrows connect the pAID side signal to the DNA side signal in the 112-bp DNA/pAID nucleosome. The double dagger (‡) indicates Lys36, which was followed by an additional tryptophan residue in the H3 peptide (differing from Lys37 in the native sequence of H3), and for which the chemical shift values could not be correctly compared with those in the 112-bp DNA/pAID nucleosome.

(C) Expanded regions of the superposition are shown for the comparison of selected residues.

(D) Chemical shift differences (Δδ) between the pAID side H3 N-tail and the DNA side H3 N-tail (black) or the H3 peptide upon 10-fold DNA (red) or pAID (cyan) addition. Chemical shift differences are plotted against residue numbers of H3

Figure 6. *Continued*
N-tails. Asterisks (*) indicate residues that were either not observed or not assigned. The dagger (†) indicates Arg2, for which the chemical shift differences were calculated by using the nominal definition of the right and left signals in Figure S2D as the DNA and the pAID sides, respectively. The double dagger (‡) indicates Lys36, which was followed by an additional tryptophan residue in the H3 peptide (differing from Lys37 in the native sequence of H3), and for which the chemical shift values could not be correctly compared with those in the 112-bp DNA/pAID nucleosome.
See also Figures S4–S6.

side signal (Figure 5D). It took approximately 64 h for the DNA side signal for Lys14 to convert to the acetylated signal (Figure 5A). Unexpectedly, the Lys14 signal in the 145-bp nucleosome was converted only to a degree of 0.3–0.4 in signal intensity ratio after 64 h (Figures 5B and 5D), although the chemical shift values of Lys14 residues in the 145-bp and 112-bp DNA/pAID nucleosomes were very similar to each other (Figures 2B, 5A, and 5B). In addition, we examined acetylation of the 145-bp nucleosome under conditions of 200 mM NaCl. Because high ionic strength is reported to reduce the catalytic activity of Gcn5 (Tanner et al., 2000), using the H3 peptide as a substrate, we confirmed that Lys14 acetylation was slower at 200 mM than at 0 mM NaCl (Figure S3B). Nevertheless, acetylation of the 145-bp nucleosome was much faster at 200 mM NaCl (Figures 5B–5D). After 11 h, the Lys14 signal was completely converted to the acetylated signal at 200 mM NaCl (Figure 5C). The acetylation rate at 200 mM NaCl roughly corresponds to that of the pAID side in the 112-bp DNA/pAID nucleosome at 0 mM NaCl (Figure 5D). These results suggest that Lys14 in the H3 N-tail on the pAID side is more exposed and accessible to Gcn5, whereas this residue both on the DNA side and in the 145-bp nucleosome is much less accessible to enzyme.

We also performed a fluorescent HAT assay of the different nucleosomal complexes (Figures S3C and S3D) under conditions similar to those of the NMR assay using Gcn5 (Figure 5E). The hFACT proteins formed complexes with the 112-bp nucleosome, but barely interacted with the intact 145-bp nucleosome (Figures S3C and S3D), consistent with previous results (Mayanagi et al., 2019; McCullough et al., 2018; Safina et al., 2017; Tsunaka et al., 2016; Valieva et al., 2017). The 112-bp DNA/pAID nucleosome was more highly acetylated when compared with the 145-bp nucleosome alone and its mixture with pAID. These findings were in good agreement with the NMR data (Figure 5D). The 112-bp nucleosome complexed with full-length hFACT was also more efficiently acetylated relative to the 145-bp nucleosomal mixture with hFACT and hFACT alone (Figure 5E), indicating that the exposed H3 tail that is accessible to Gcn5 is also induced by full-length hFACT, similar to pAID alone.

Environmental Differences between DNA- or pAID-Bound H3 Peptide and H3 N-Tails in the 112-bp DNA/pAID Nucleosome

To further clarify the distinct chemical environments around the two H3 N-tails in the 112-bp DNA/pAID nucleosome, we measured the ^{1}H-^{15}N HSQC spectrum of an isolated ^{15}N-peptide comprising H3 N-tail residues Ala1–Lys36 plus an additional Trp37 residue to allow quantitative estimation. NMR signals were hardly observed for the free peptide under the same conditions used for the nucleosomes (20 mM HEPES-NaOH, pH 7.0, 293K) (Figure S4A), presumably because of fast exchange between the amide protons and solvent. Some signals appeared upon the addition of 20 mM Na/K phosphate buffer, pH 7.0, because the exchange rates are likely to be slower in a phosphate environment, which may mimic the DNA phosphate backbone (Figure S4B). Likewise, signals from each residue of the H3 peptide appeared after the addition of a 0.25-fold amount of 33-bp 601 DNA or pAID protein (Figures S5A and S5B), owing to the slower exchange rate caused by dynamic interactions with DNA or pAID. After a 10-fold addition of DNA or pAID, further changes in chemical shift and signal intensity were not clearly observed (Figure S6A and S6B), suggesting that a small addition of DNA or pAID is sufficient for dynamic interaction with the H3 peptide.

The conformations of the H3 peptide bound to either DNA or pAID, and the two H3 tails within the 112-bp DNA/pAID nucleosome were compared by superposition of the corresponding ^{1}H-^{15}N HSQC spectra (Figures 6A, 6B, S6C, and S6D). Signals for Lys4, Thr6–Lys9, Gly12, Lys14, Arg17, Gln19–Ala21, Lys23–Ala29, and Thr32–Gly34 of the DNA- or pAID-bound H3 peptide were observed along a near-linear trajectory between the pAID and DNA side signals in the 112-bp DNA/pAID nucleosome (Figures 6A–6C). The chemical shift changes between the DNA- or pAID-bound H3 peptide and the pAID side H3 N-tail were significantly smaller than the changes between the DNA and pAID side H3 N-tails (Figure 6D). These results suggest that the pAID side H3 tail dynamically interacts with DNA or pAID in the same manner as the respective DNA- or pAID-bound H3 peptide, whereas the DNA side H3 tail more closely interacts with DNA when

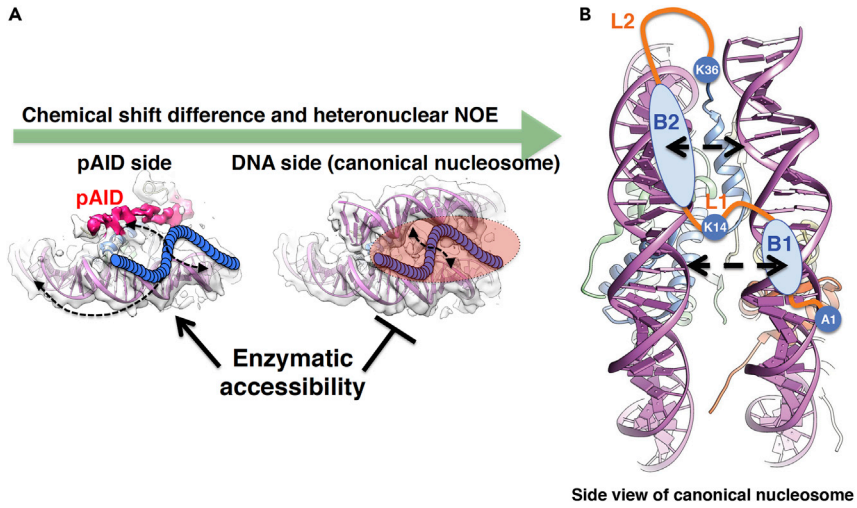

Figure 7. Summary of the Dynamic Conformations of the Nucleosomal H3 N-Tails

(A) Dynamic structures of two H3 N-tails in the 112-bp DNA/pAID nucleosome. Two views of the EM density map (EMD-9639) on the nucleosome structure (PDB: 2CV5), colored as in Figure 1B, are shown. Blue circular chains denote the H3 N-tails. Dotted arrows represent the dynamic behavior of the H3 N-tails. The dashed ellipsoid, shaded in red, represents the space between two DNA gyres within the canonical nucleosome or on the DNA side in the 112-bp DNA/pAID nucleosome.

(B) DNA-binding model of H3 N-tails in the canonical nucleosome. A side view of the nucleosome structure (PDB: 2CV5), colored as in Figure 1B, is shown. Blue ellipsoids represent the two basic segments, B1 and B2, in the H3 N-tail. Orange strings represent the linkers, L1 and L2, in the H3 N-tail. Dotted arrows represent the dynamic behavior of the H3 N-tails. See also Figure S7.

compared with the DNA-bound H3 peptide. As shown in Figures 7A and S7, the DNA side H3 N-tail might be dynamically but restrictedly localized to a minor space between two DNA gyres. This localization probably inhibits the accessibility of Gcn5 to Lys14 on the DNA side.

Local Conformations of H3 N-Tails in the 145-bp Nucleosome

The location of the DNA side H3 N-tail in the 112-bp DNA/pAID nucleosome structurally corresponds to the location of the H3 N-tail in the canonical nucleosome (Figures 7A and 7B). The similarity in chemical shift and NOE values of the DNA side and 145-bp nucleosome H3 N-tails (Figures 2B, 4C, and 4D) also indicated that the H3 N-tails in the 145-bp nucleosome are likely to localize dynamically into two DNA gyres. The pattern of chemical shift changes of H3 N-tails in the 145-bp nucleosome upon NaCl titration (Figure 4B) indicated that electrostatic interactions between the H3 N-tails and two DNA gyres extensively affect the dynamic motion of the whole H3 N-tails. The B2 segment within the H3 N-tails showed relatively high NOE values (Figure 4D) and large chemical shift changes upon NaCl titration (Figure 4B). The B1 segment also showed high NOE values and chemical shift changes (Figures 4B and 4D), suggesting that both B1 and B2 are responsible for interaction with the two DNA gyres (Figure 7B).

The L1 linker connecting B1 and B2 showed smaller chemical shift changes upon NaCl titration when compared with average values (Figure 4B) and relatively high NOE values (Figure 4D), suggesting that it may not directly interact with DNA, but is indirectly confined to two DNA gyres (Figure 7B). In the crystal structures of *Tetrahymena* Gcn5 bound to an H3 peptide, the Gcn5 HAT domain mainly recognizes L1 containing Lys14 and Pro16–Gln19 of B2 (Clements et al., 2003; Rojas et al., 1999). L1 and part of B2, confined to two DNA gyres, are more likely to inhibit the acetylation of Lys14 by Gcn5 (Figure 7B). In particular, Ser10–Lys14 of L1 in the 145-bp nucleosome showed higher NOE values when compared with the corresponding residues on the DNA side (Figures 4C and 4D). This indicates that L1 in the 145-bp nucleosome is restricted more tightly to the two DNA gyres when compared with L1 on the DNA side in the 112-bp DNA/pAID nucleosome; thus, the accessibility of Gcn5 to Lys14 is even further inhibited in 145-bp nucleosome. In fact, the H3 acetylation rate was much slower in the 145-bp nucleosome than on the DNA side in the 112-bp DNA/pAID nucleosome (Figures 5A, 5B, and 5D). In contrast, L2 showed much lower NOE values

and chemical shift changes when compared with other residues (Figures 4B and 4D), confirming the relatively higher mobility of this linker.

DISCUSSION

The present NMR analysis has verified the presence of distinct chemical environments around the two H3 N-tails in the 112-bp DNA/pAID nucleosome (Figures 1B, 2A, 2B, 3A, and 3B). These chemical environments were compared with those of the isolated H3 peptide bound to a DNA oligomer or the pAID protein (Figures 6A, 6B, S6C, and S6D). The basic H3 peptide dynamically interacted with phosphate groups on DNA and pAID (Figures S6A and S6B). The smaller chemical shift changes between the H3 peptide bound to DNA or pAID and the H3 N-tail on the pAID side in the 112-bp DNA/pAID nucleosome (Figure 6D) indicate that the dynamic behavior of the H3 peptide is similar to that of the pAID side H3 N-tail in the interaction with DNA or pAID. In analogy with this, previous studies of the canonical nucleosome using molecular dynamics simulations suggested that the nucleosomal H3 N-tails dynamically collapse onto the surrounding DNA duplex (Morrison et al., 2018; Shaytan et al., 2016). Here, however, the H3 N-tails on the DNA side and in the 145-bp nucleosome exhibited substantial changes in chemical shift when compared with the pAID side H3 N-tail (Figures 2B and 6A–6D). This difference presumably originates from the different interaction targets of the pAID and DNA side H3 N-tails. The DNA side H3 N-tail is likely to favor the two DNA duplexes around the DNA side (Figure S7, DNA side view) rather than the single DNA duplex around the dyad axis (Figure S7, top view). By contrast, the H3 N-tail on the pAID side may interact in a state of dynamic equilibrium across one DNA duplex around the dyad axis (Figure S7, top view) and one DNA duplex or one pAID segment around the pAID side (Figure S7, pAID side view). This change in the dynamic behavior of the tail might make it more sensitive to the HAT activity of Gcn5 (Figures 5D and 5E).

In the acetylation reaction of the unmodified nucleosomal complexes, it took 11–64 h to acetylate H3 Lys14 using Gcn5 (Figure 5D). By contrast, in the reaction of the H3 peptide with a 0.25-fold amount of 33-bp DNA, it took only 1 h to acetylate Lys14 under the same conditions (Figure S3B). These results indicate that relatively tight contacts between the histone tails and DNA within nucleosome substantially inhibit enzymatic accessibility to the H3 N-tails. *In vivo*, however, there should be various regulatory mechanisms that increase H3 N-tail accessibility to HAT. In fact, the bromodomain within full-length Gcn5 interacts with acetylated histone H4 in nucleosome, thereby facilitating H3 N-tail acetylation by Gcn5 (Li and Shogren-Knaak, 2009). The interaction of nucleosome with hFACT might also enhance acetylation. Therefore, it is likely that *in vivo* epigenetic processes are much more efficient than the *in vitro* reaction.

It has been reported that the H3 N-tails in the 147-bp nucleosome prevent nucleosome association with a PHD finger domain, whereas charge-modulating mutations or modifications of the H3 N-tails that weaken the interaction with DNA increase domain binding (Morrison et al., 2018). This finding is in agreement with our results showing that the H3 N-tails in the 145-bp nucleosome are protected from Gcn5, but partial replacement of the nucleosomal DNA with hFACT increases Gcn5 accessibility to the H3 N-tails (Figures 5D, 5E, 7A, and 7B). In addition, replacement of DNA with hFACT may recruit effector domains located in ATP-dependent chromatin remodeling complexes (Clapier et al., 2017) to the H3 N-tail released from DNA in the complex. In fact, FACT recruits the Polybromo-associated Brm (PBAP) remodeler, which belongs to the SWI/SNF-type of complexes with bromodomains, to the chromatin boundaries, thereby counteracting the spreading of heterochromatin in *Drosophila* (Nakayama et al., 2012).

A recent study revealed that FACT, localized to heterochromatin, prevents histone turnover at closed chromatin sites with high nucleosome occupancy in *S. pombe* (Holla et al., 2020). This highlights our previous EM structures, which showed that the replacement of DNA with pAID prevents histone loss (Mayanagi et al., 2019). We envisage that the replacement of DNA with pAID may be an initial step to enable hFACT to invade the condensed chromatin structure. Considering that the H3 tail is more exposed to solvent (Figure 7A), invasion of hFACT may be a potential trigger for converting inactive chromatin regions to a more open structure. In fact, several studies have reported that FACT promotes the expression of key proteins that are repressed in heterochromatin. FACT facilitates DNA demethylation at heterochromatic transposable elements in *Arabidopsis* (Frost et al., 2018) and is required for efficient expression of DOG1, which is involved in the switch from seed dormancy to germination in *Arabidopsis* (Michl-Holzinger et al., 2019).

Last, mammalian FACT depletion inhibits the induction of pluripotency in reprogramming (Shen et al., 2018).

In summary, our NMR analyses have enabled us to propose an advanced model, in which the partial replacement of nucleosomal DNA with hFACT acts as a modulator for dynamic behavior of the H3 tails, thereby altering their accessibility to HAT (Figures 7A and S7). This finding underscores the strong correlation between the dynamic state of histone tails in unwrapped nucleosomes and protein accessibility. Modulation of the dynamic behavior of histone tails is one of the universal determinants of hierarchical chromatin structures. In future studies, therefore, it will be essential to examine the dynamic structures of histone tails within nucleosomes unwrapped by histone variants, chromatin remodelers, RNA polymerase II, and pioneer factors, among many others (Brahma and Henikoff, 2020; Dodonova et al., 2020; Ehara et al., 2019; Farnung et al., 2017; He et al., 2020; Kujirai et al., 2018; Michael et al., 2020; Ramachandran et al., 2017; Sinha et al., 2017; Tachiwana et al., 2011). It should be stressed that NMR analysis is the only method currently available to directly measure the chemical environment around the histone tail within such multiple protein complexes, which are likely to be essential for epigenetic regulation and chromatin remodeling.

Limitation of the Study

The major significance of our study using hFACT is mostly based on structural biology and *in vitro* biochemical data. Additional *in vivo* data would be required in future works. However, amino acid sequences within pAID are less conserved between yeast and human. Therefore, any mutational experiments within pAID, using yeast, may not lead to correct interpretation of hFACT functions.

Resource Availability

Lead Contact

Further information and requests for resources and reagents should be directed to and will be fulfilled by the Lead Contact, Dr. Yoshifumi Nishimura (nisimura@yokohama-cu.ac.jp).

Materials Availability

This study did not generate new unique reagents.

Data and Code Availability

The datasets supporting the current study have not been deposited in a public repository but are available from the corresponding author on request.

METHODS

All methods can be found in the accompanying Transparent Methods supplemental file.

SUPPLEMENTAL INFORMATION

Supplemental Information can be found online at https://doi.org/10.1016/j.isci.2020.101641.

ACKNOWLEDGMENTS

The authors are grateful to Dr. Kyohei Arita for their kind gift of the expression vector that generated the H3 peptide. This work was supported in part by a Grants-in-Aid for Scientific Research (C) (JSPS KAKENHI grant no. JP18K06064 [to Y.T.]). This work was partly supported by Grants-in-Aid for Scientific Research on an NMR platform (07022019) (to Y.N.) from the Ministry of Education, Culture, Sports, Science and Technology (MEXT), Japan and Platform Project for Supporting Drug Discovery and Life Science Research (Basis for Supporting Innovative Drug Discovery and Life Science Research [BINDS]) from the Japan Agency for Medical Research and Development (AMED) (Grant Number JP18am0101033 [*support number 0004*] [to Y.N.]).

AUTHORS CONTRIBUTIONS

Conceptualization, Y.T. and Y.N.; Sample Preparation, Y.T and H.O.; Methodology, Y.T., H.O., and Y.N.; Investigation, Y.T. and H.O.; Writing – Original Draft, Y.T.; Writing – Review & Editing, H.O., K.M., and Y.N; Funding Acquisition, Y.T. and Y.N.; Resources, Y.T., K.M., and Y.N.; Supervision, Y.N.

DECLARATION OF INTERESTS

The authors declare no competing interests.

Received: July 10, 2020
Revised: September 9, 2020
Accepted: September 29, 2020
Published: October 23, 2020

REFERENCES

Andresen, K., Jimenez-Useche, I., Howell, S.C., Yuan, C., and Qiu, X. (2013). Solution scattering and FRET studies on nucleosomes reveal DNA unwrapping effects of H3 and H4 tail removal. PLoS One *8*, e78587.

Andrews, F.H., Strahl, B.D., and Kutateladze, T.G. (2016). Insights into newly discovered marks and readers of epigenetic information. Nat. Chem. Biol. *12*, 662–668.

Armache, J.P., Gamarra, N., Johnson, S.L., Leonard, J.D., Wu, S., Narlikar, G.J., and Cheng, Y. (2019). Cryo-EM structures of remodeler-nucleosome intermediates suggest allosteric control through the nucleosome. Elife *8*, e46057.

Bannister, A.J., and Kouzarides, T. (2011). Regulation of chromatin by histone modifications. Cell Res. *21*, 381–395.

Belotserkovskaya, R., Oh, S., Bondarenko, V.A., Orphanides, G., Studitsky, V.M., and Reinberg, D. (2003). FACT facilitates transcription-dependent nucleosome alteration. Science *301*, 1090–1093.

Brahma, S., and Henikoff, S. (2020). Epigenome regulation by dynamic nucleosome unwrapping. Trends Biochem. Sci. *45*, 13–26.

Chi, P., Allis, C.D., and Wang, G.G. (2010). Covalent histone modifications — miswritten, misinterpreted and mis-erased in human cancers. Nat. Rev. Cancer *10*, 457–469.

Clapier, C.R., Iwasa, J., Cairns, B.R., and Peterson, C.L. (2017). Mechanisms of action and regulation of ATP-dependent chromatin-remodelling complexes. Nat. Rev. Mol. Cell Biol. *18*, 407–422.

Clements, A., Poux, A.N., Lo, W.-S., Pillus, L., Berger, S.L., and Marmorstein, R. (2003). Structural basis for histone and phosphohistone binding by the GCN5 histone acetyltransferase. Mol. Cell *12*, 461–473.

Dodonova, S.O., Zhu, F., Dienemann, C., Taipale, J., and Cramer, P. (2020). Nucleosome-bound SOX2 and SOX11 structures elucidate pioneer factor function. Nature *580*, 669–672.

Ehara, H., Kujirai, T., Fujino, Y., Shirouzu, M., Kurumizaka, H., and Sekine, S.-I. (2019). Structural insight into nucleosome transcription by RNA polymerase II with elongation factors. Science *363*, 744–747.

Farnung, L., Vos, S.M., Wigge, C., and Cramer, P. (2017). Nucleosome–Chd1 structure and implications for chromatin remodelling. Nature *550*, 539–542.

Frost, J.M., Kim, M.Y., Park, G.T., Hsieh, P.-H., Nakamura, M., Lin, S.J.H., Yoo, H., Choi, J., Ikeda, Y., Kinoshita, T., et al. (2018). FACT complex is required for DNA demethylation at heterochromatin during reproduction in Arabidopsis. Proc. Natl. Acad. Sci. U S A *115*, E4720–E4729.

He, S., Wu, Z., Tian, Y., Yu, Z., Yu, J., Wang, X., Li, J., Liu, B., and Xu, Y. (2020). Structure of nucleosome-bound human BAF complex. Science *367*, 875–881.

Holla, S., Dhakshnamoorthy, J., Folco, H.D., Balachandran, V., Xiao, H., Sun, L.-L., Wheeler, D., Zofall, M., and Grewal, S.I.S. (2020). Positioning heterochromatin at the nuclear periphery suppresses histone turnover to promote epigenetic inheritance. Cell *180*, 150–164.

Iwasaki, W., Miya, Y., Horikoshi, N., Osakabe, A., Taguchi, H., Tachiwana, H., Shibata, T., Kagawa, W., and Kurumizaka, H. (2013). Contribution of histone N-terminal tails to the structure and stability of nucleosomes. FEBS Open Biol. *3*, 363–369.

Kato, D., Osakabe, A., Arimura, Y., Mizukami, Y., Horikoshi, N., Saikusa, K., Akashi, S., Nishimura, Y., Park, S.-Y., Nogami, J., et al. (2017). Crystal structure of the overlapping dinucleosome composed of hexasome and octasome. Science *356*, 205–208.

Klemm, S.L., Shipony, Z., and Greenleaf, W.J. (2019). Chromatin accessibility and the regulatory epigenome. Nat. Rev. Genet. *20*, 207–220.

Kujirai, T., Ehara, H., Fujino, Y., Shirouzu, M., Sekine, S.-I., and Kurumizaka, H. (2018). Structural basis of the nucleosome transition during RNA polymerase II passage. Science *362*, 595–598.

Lai, W.K.M., and Pugh, B.F. (2017). Understanding nucleosome dynamics and their links to gene expression and DNA replication. Nat. Rev. Mol. Cell Biol. *18*, 548–562.

Li, S., and Shogren-Knaak, M.A. (2009). The Gcn5 bromodomain of the SAGA complex facilitatescooperative and cross-tail acetylation of nucleosomes. J. Biol. Chem. *284*, 9411–9417.

Liu, Y., Zhou, K., Zhang, N., Wei, H., Tan, Y.Z., Zhang, Z., Carragher, B., Potter, C.S., D'Arcy, S., and Luger, K. (2020). FACT caught in the act of manipulating the nucleosome. Nature *577*, 426–431.

Luger, K., Mader, A., Richmond, R.K., Sargent, D.F., and Richmond, T.J. (1997). Crystal structure of the nucleosome core particle at 2.8 Å resolution. Nature *389*, 251–260.

Mayanagi, K., Saikusa, K., Miyazaki, N., Akashi, S., Iwasaki, K., Nishimura, Y., Morikawa, K., and Tsunaka, Y. (2019). Structural visualization of key steps in nucleosome reorganization by human FACT. Sci. Rep. *9*, 10183.

McCullough, L., Connell, Z., Xin, H., Studitsky, V.M., Feofanov, A.V., Valieva, M.E., and Formosa, T. (2018). Functional roles of the DNA-binding HMGB domain in the histone chaperone FACT in nucleosome reorganization. J. Biol. Chem. *293*, 6121–6133.

Michael, A.K., Grand, R.S., Isbel, L., Cavadini, S., Kozicka, Z., Kempf, G., Bunker, R.D., Schenk, A.D., Graff-Meyer, A., Pathare, G.R., et al. (2020). Mechanisms of OCT4-SOX2 motif readout on nucleosomes. Science *368*, 1460–1465.

Michl-Holzinger, P., Mortensen, S.A., and Grasser, K.D. (2019). The SSRP1 subunit of the histone chaperone FACT is required for seed dormancy in Arabidopsis. J. Plant Physiol. *236*, 105–108.

Morrison, E.A., Bowerman, S., Sylvers, K.L., Wereszczynski, J., and Musselman, C.A. (2018). The conformation of the histone H3 tail inhibits association of the BPTF PHD finger with the nucleosome. Elife *7*, e31481.

Musselman, C.A., Lalonde, M.-E., Côté, J., and Kutateladze, T.G. (2012). Perceiving the epigenetic landscape through histone readers. Nat. Struct. Mol. Biol. *19*, 1218–1227.

Nakayama, T., Nishioka, K., Dong, Y.-X., Shimojima, T., and Hirose, S. (2007). Drosophila GAGA factor directs histone H3.3 replacement that prevents the heterochromatin spreading. Genes Dev. *21*, 552–561.

Nakayama, T., Shimojima, T., and Hirose, S. (2012). The PBAP remodeling complex is required for histone H3.3 replacement at chromatin boundaries and for boundary functions. Development *139*, 4582–4590.

Pettersen, E.F., Goddard, T.D., Huang, C.C., Couch, G.S., Greenblatt, D.M., Meng, E.C., and Ferrin, T.E. (2004). UCSF Chimera - a visualization system for exploratory research and analysis. J. Comput. Chem. *25*, 1605–1612.

Ramachandran, S., Ahmad, K., and Henikoff, S. (2017). Transcription and remodeling produce asymmetrically unwrapped nucleosomal intermediates. Mol. Cell *68*, 1038–1053.

Rojas, J.R., Trievel, R.C., Zhou, J., Mo, Y., Li, X., Berger, S.L., and Marmorstein, C.D.A.R. (1999). Structure of Tetrahymena GCN5 bound to coenzyme A and a histone H3 peptide. Nature *401*, 93–98.

Safina, A., Cheney, P., Pal, M., Brodsky, L., Ivanov, A., Kirsanov, K., Lesovaya, E., Naberezhnov, D., Nesher, E., Koman, I., et al. (2017). FACT is a

sensor of DNA torsional stress in eukaryotic cells. Nucleic Acids Res. *45*, 1925–1945.

Shaytan, A.K., Armeev, G.A., Goncearenco, A., Zhurkin, V.B., Landsman, D., and Panchenko, A.R. (2016). Coupling between histone conformations and DNA geometry in nucleosomes on a microsecond timescale: atomistic insights into nucleosome functions. J. Mol. Biol. *428*, 221–237.

Shen, Z., Formosa, T., and Tantin, D. (2018). FACT inhibition blocks induction but not maintenance of pluripotency. Stem Cells Dev. *27*, 1693–1701.

Sinha, K.K., Gross, J.D., and Narlikar, G.J. (2017). Distortion of histone octamer core promotes nucleosome mobilization by a chromatin remodeler. Science *355*, eaaa3761.

Stewart-Morgan, K.R., Petryk, N., and Groth, A. (2020). Chromatin replication and epigenetic cell memory. Nat. Cell Biol. *22*, 361–371.

Stützer, A., Liokatis, S., Kiesel, A., Schwarzer, D., Sprangers, R., Söding, J., Selenko, P., and Fischle, W. (2016). Modulations of DNA contacts by linker histones and post-translational modifications determine the mobility and modifiability of nucleosomal H3 tails. Mol. Cell *61*, 247–259.

Suganuma, T., and Workman, J.L. (2011). Signals and combinatorial functions of histone modifications. Annu. Rev. Biochem. *80*, 473–499.

Tachiwana, H., Kagawa, W., Shiga, T., Osakabe, A., Miya, Y., Saito, K., Hayashi-Takanaka, Y., Oda, T., Sato, M., Park, S.-Y., et al. (2011). Crystal structure of the human centromeric nucleosome containing CENP-A. Nature *476*, 232–235.

Tanner, K.G., Langer, M.R., Kim, Y., and Denu, J.M. (2000). Kinetic mechanism of the histone acetyltransferase GCN5 from yeast. J. Biol. Chem. *275*, 22048–22055.

Tsunaka, Y., Fujiwara, Y., Oyama, T., Hirose, S., and Morikawa, K. (2016). Integrated molecular mechanism directing nucleosome reorganization by human FACT. Genes Dev. *30*, 673–686.

Tsunaka, Y., Kajimura, N., Tate, S., and Morikawa, K. (2005). Alteration of the nucleosomal DNA path in the crystal structure of a human nucleosome core particle. Nucleic Acids Res. *33*, 3424–3434.

Valieva, M.E., Gerasimova, N.S., Kudryashova, K.S., Kozlova, A.L., Kirpichnikov, M.P., Hu, Q., Botuyan, M.V., Mer, G., Feofanov, A.V., and Studitsky, V.M. (2017). Stabilization of nucleosomes by histone tails and by FACT revealed by spFRET microscopy. Cancers (Basel) *9*, 3.

Vasudevan, D., Chua, E.Y.D., and Davey, C.A. (2010). Crystal structures of nucleosome core particles containing the "601" strong positioning sequence. J. Mol. Biol. *403*, 1–10.

Zentner, G.E., and Henikoff, S. (2013). Regulation of nucleosome dynamics by histone modifications. Nat. Struct. Mol. Biol. *20*, 259–266.

Zhou, B.-R., Feng, H., Ghirlando, R., Kato, H., Gruschus, J., and Bai, Y. (2012). Histone H4 K16Q mutation, an acetylation mimic, causes structural disorder of its n-terminal basic patch in the nucleosome. J. Mol. Biol. *421*, 30–37.

iScience, Volume *23*

Supplemental Information

Partial Replacement of Nucleosomal DNA with Human FACT Induces Dynamic Exposure and Acetylation of Histone H3 N-Terminal Tails

Yasuo Tsunaka, Hideaki Ohtomo, Kosuke Morikawa, and Yoshifumi Nishimura

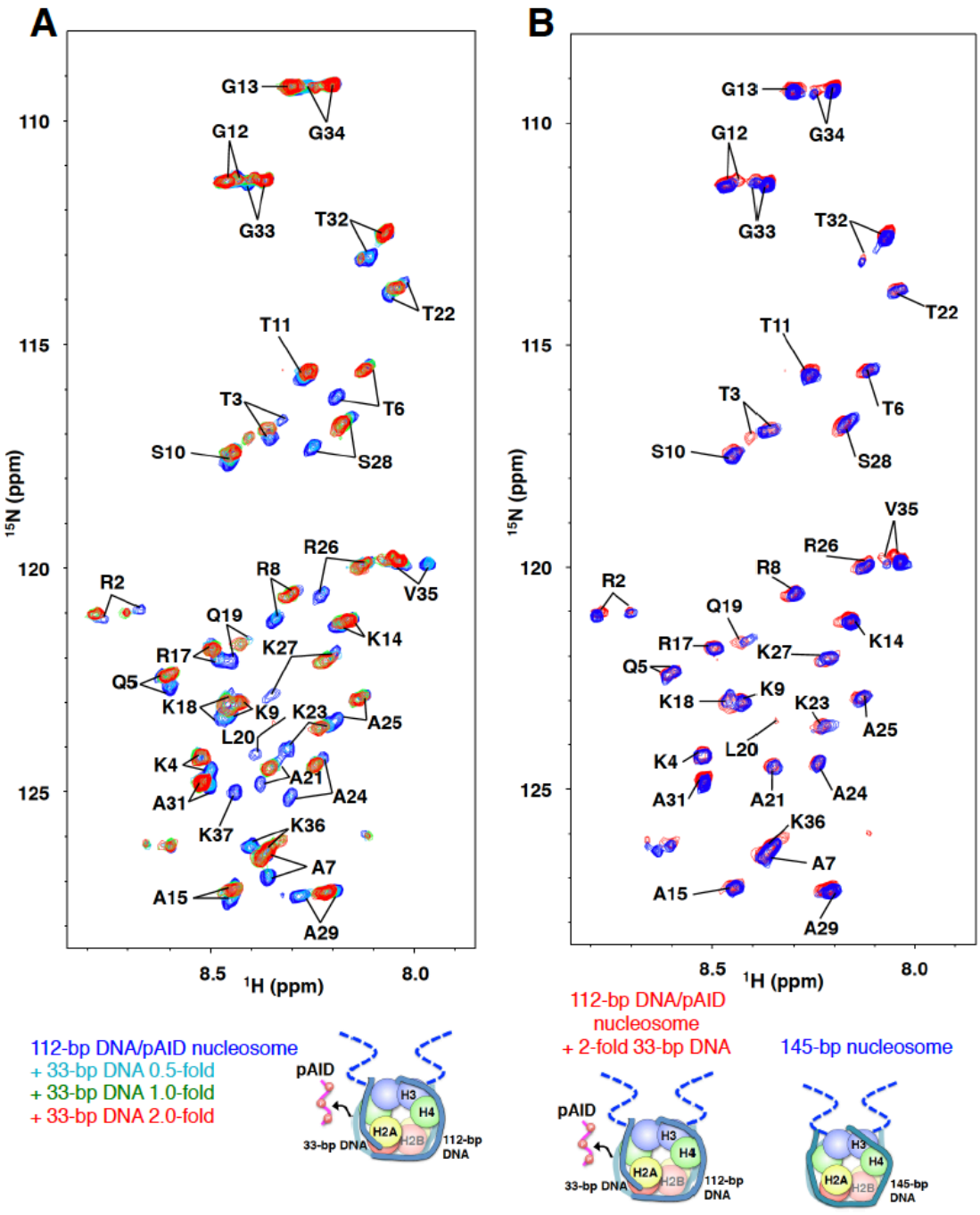

Figure S1. Related to Figure 2. NMR spectra of the 112-bp DNA/pAID nucleosome upon titration with 33-bp DNA.

(**A**) Spectral superposition of the 2D ^{1}H-^{15}N HSQC spectra of the 112-bp DNA/pAID nucleosome upon titration with 33-bp DNA at molar ratios of 1:0 (blue), 1:0.5 (cyan), 1:1 (green), and 1:2 (red). Signal assignments in the 112-bp DNA/pAID nucleosome are labeled. Cartoon models of the nucleosomal

complexes are below, colored as in Figure 2A.

(**B**) Spectral comparison of 2D ^{1}H-^{15}N HSQC spectra between the 145-bp nucleosome (blue) and the 112-bp DNA/pAID nucleosome upon the addition of a two-fold excess of DNA (red). Signal assignments in the 112-bp DNA/pAID nucleosome upon the addition of 33-bp DNA are labeled.

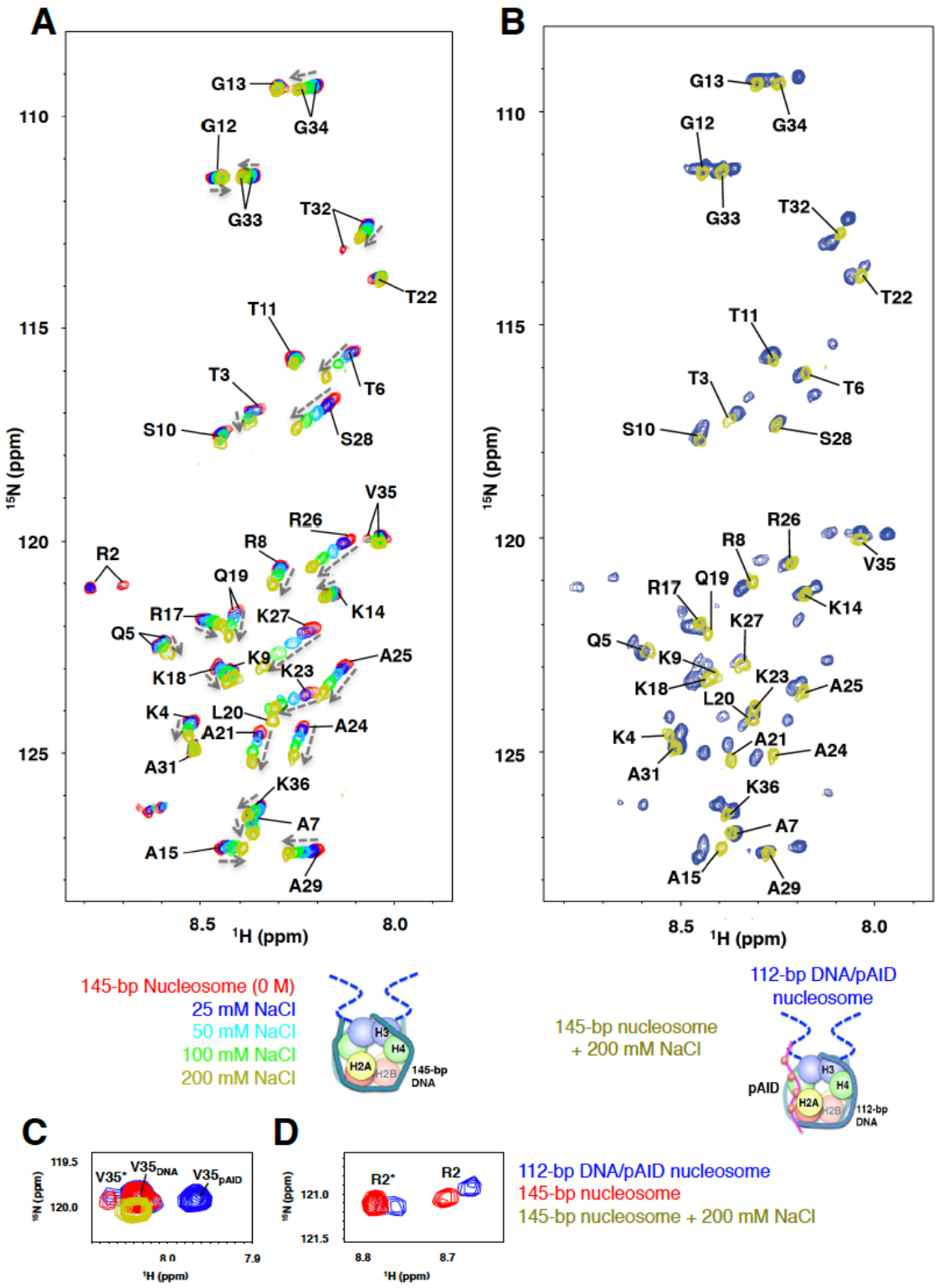

Figure S2. Related to Figure 3. NMR spectra of the 145-bp nucleosome upon titration with NaCl.

(**A**) Spectral superposition of 2D ^{1}H-^{15}N HSQC spectra of the 145-bp

nucleosome upon NaCl titration at 0 M (red), 25 mM (blue), 50 mM (cyan), 100 mM (green), and 200 mM (yellow). Signal assignments in the 145-bp nucleosome at 0 mM NaCl are labeled. Cartoon models of the nucleosomal complexes are below, colored as in Figure 2A.

(**B**) Spectral comparison of 2D ^{1}H-^{15}N HSQC spectra between the 112-bp DNA/pAID nucleosome (blue) and the 145-bp nucleosome at 200 mM NaCl (yellow). The signal assignments in the 145-bp nucleosome at 200 mM NaCl are labeled.

(**C, D**) Spectral comparison of 2D ^{1}H-^{15}N HSQC spectra at Val35 (C) and Arg2 (D) for the 145-bp nucleosome (red), the 145-bp nucleosome at 200 mM NaCl (yellow), and the 112-bp DNA/pAID nucleosome (blue). Even in the 145-bp nucleosome, Arg2 exhibited two separate signals similar to Arg2 in the 112-bp DNA/pAID nucleosome. However, the two Arg2 signals disappeared upon NaCl titration. The NOE value of one signal (R2) was higher than that of the other (R2*) (Figure 4D), suggesting rigid and flexible states, respectively. The neighboring residue Thr3 was observed to have a broad signal (Figure 2B) and showed two separate signals in the 112/33-bp nucleosome (Figure S1B). Arg2 and Thr3, which are close to the N-terminus, may adopt two conformations: a DNA-binding and a more exposed conformation. Val35 had a minor signal (V35*), which partially overlapped with the DNA side signal and was apart from the pAID side signal. Thr32, Gly33, and Gly34 also harbored minor signals, roughly corresponding to the pAID side signals (Figure 2B). These minor signals were impaired (Thr32) or incorporated into the corresponding pAID side signal (Gly33 and Gly34) upon NaCl titration (Figures 2B, 3A, and S2A), suggesting that the minor conformations of Thr32, Gly33, and Gly34 in the 145-bp nucleosome are more exposed states similar to the other pAID side residues in the 112-bp DNA/pAID nucleosome.

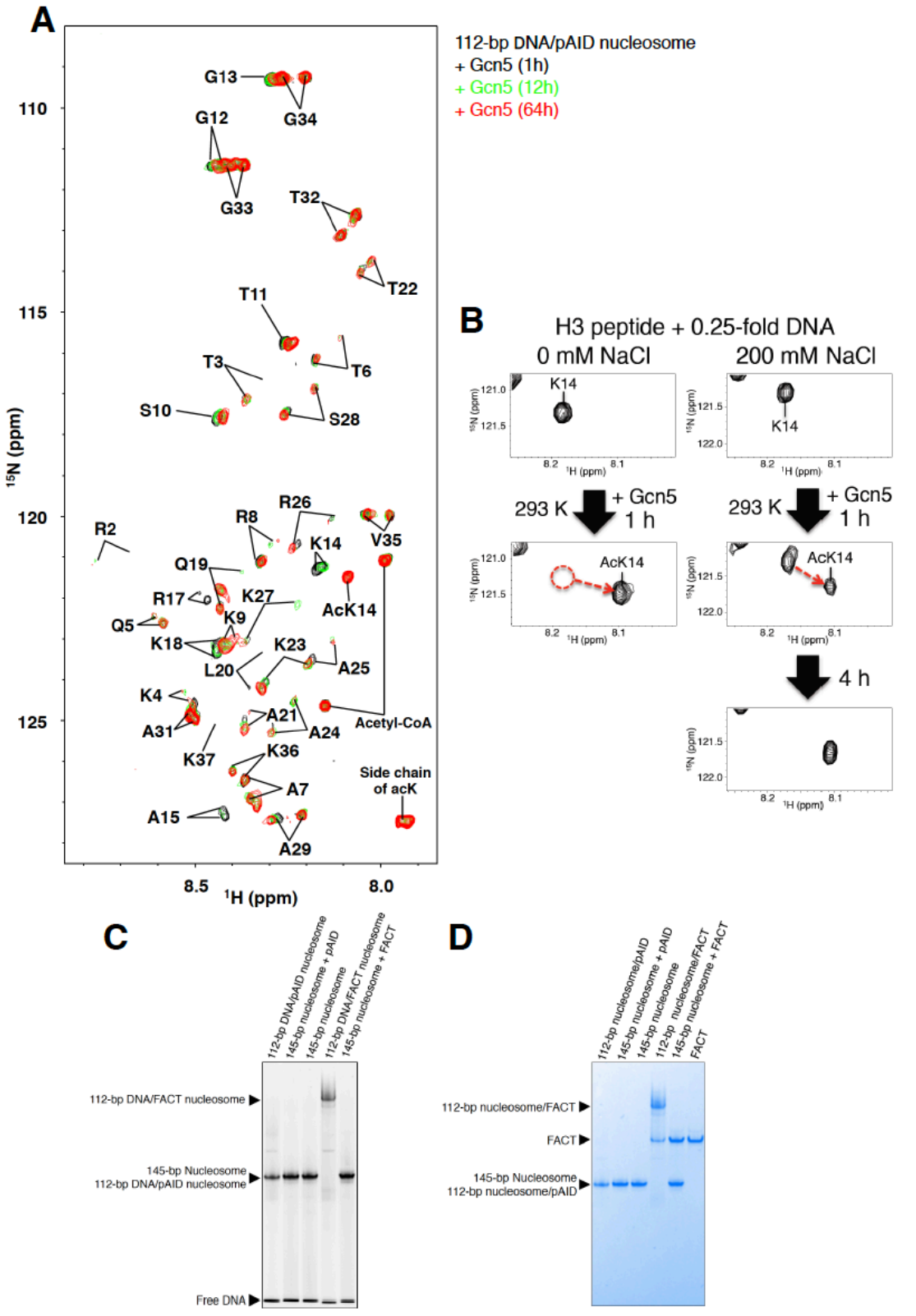

Figure S3. Related to Figure 5. Acetylation of the nucleosomal complexes by Gcn5.

(**A**) NMR spectra of the 112-bp DNA/pAID nucleosome at 1 (black), 12 (green), and 64 (red) hours after addition of Gcn5. Signal assignments in the 112-bp DNA/pAID nucleosome are labeled.

(**B**) Expanded view of the ^{1}H-^{15}N NMR spectrum at Lys14 of the H3 peptide upon a 0.25-fold addition of 33-bp DNA at 0 mM and 200 mM NaCl during acetylation by Gcn5. After 1 hour, the signal for Lys14 was completely converted to the acetylated signal at 0 mM NaCl (left panel). By contrast, it took approximately 4 hours for the Lys14 signal to convert to the acetylated signal at 200 mM NaCl (right panel). The acetylation rate of the H3 peptide was slower at 200 mM NaCl than at 0 mM NaCl.

(**C, D**) SYBR Gold-stained EMSAs (C) and the CBB-stained duplicate (D) of nucleosomal complexes before the acetylation reactions. The free pAID protein was not stained by CBB, owing to its highly negative charge cluster. Experiments were repeated at least three times.

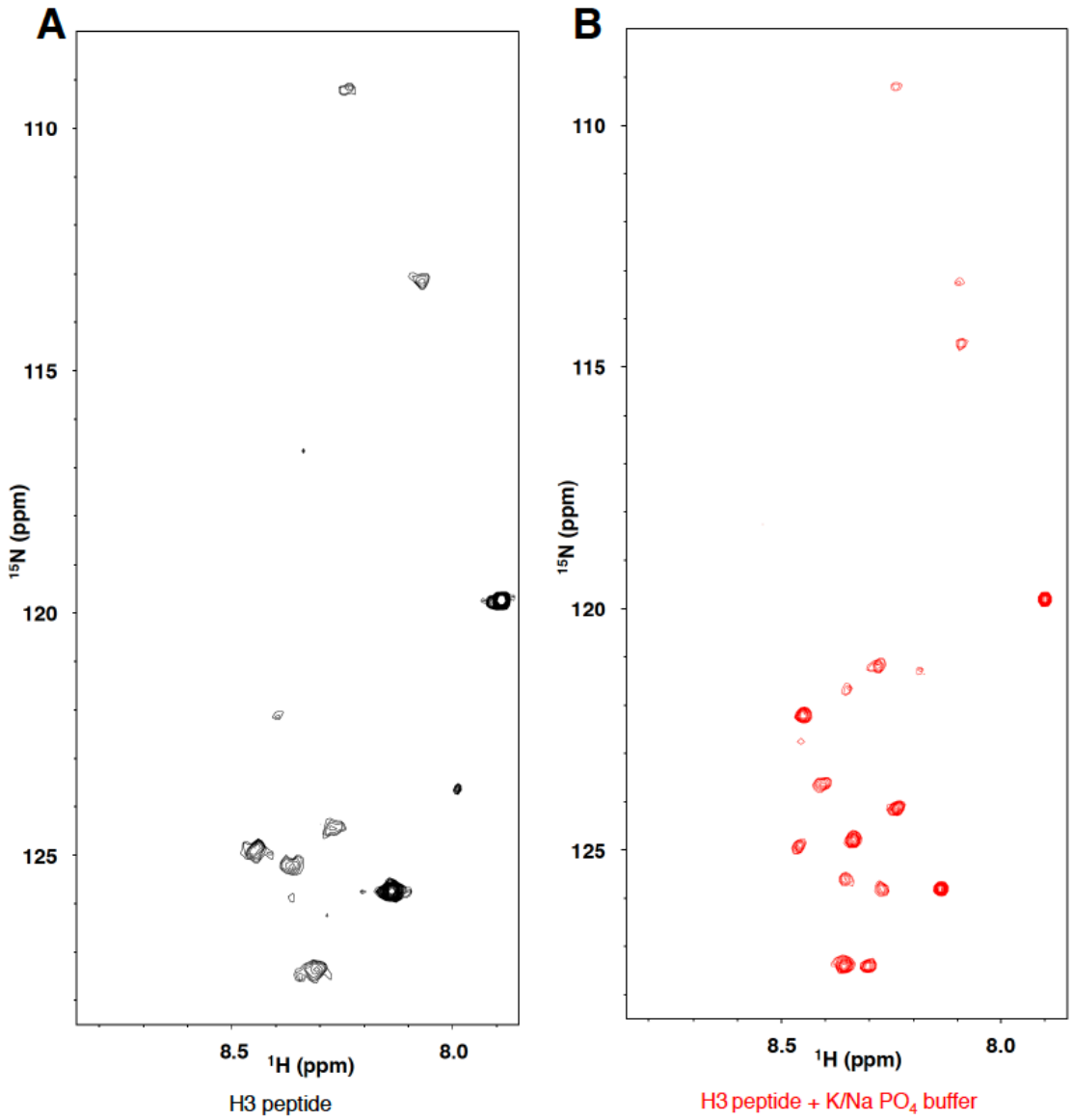

Figure S4. Related to Figure 6. NMR spectra of the free H3 peptide under different conditions.

(**A**) 2D ^{1}H-^{15}N HSQC spectrum of the H3 peptide in 20 mM HEPES-NaOH, pH 7.0.

(**B**) 2D ^{1}H-^{15}N HSQC spectrum of the H3 peptide upon the addition of 20 mM Na/K phosphate buffer, pH 7.0.

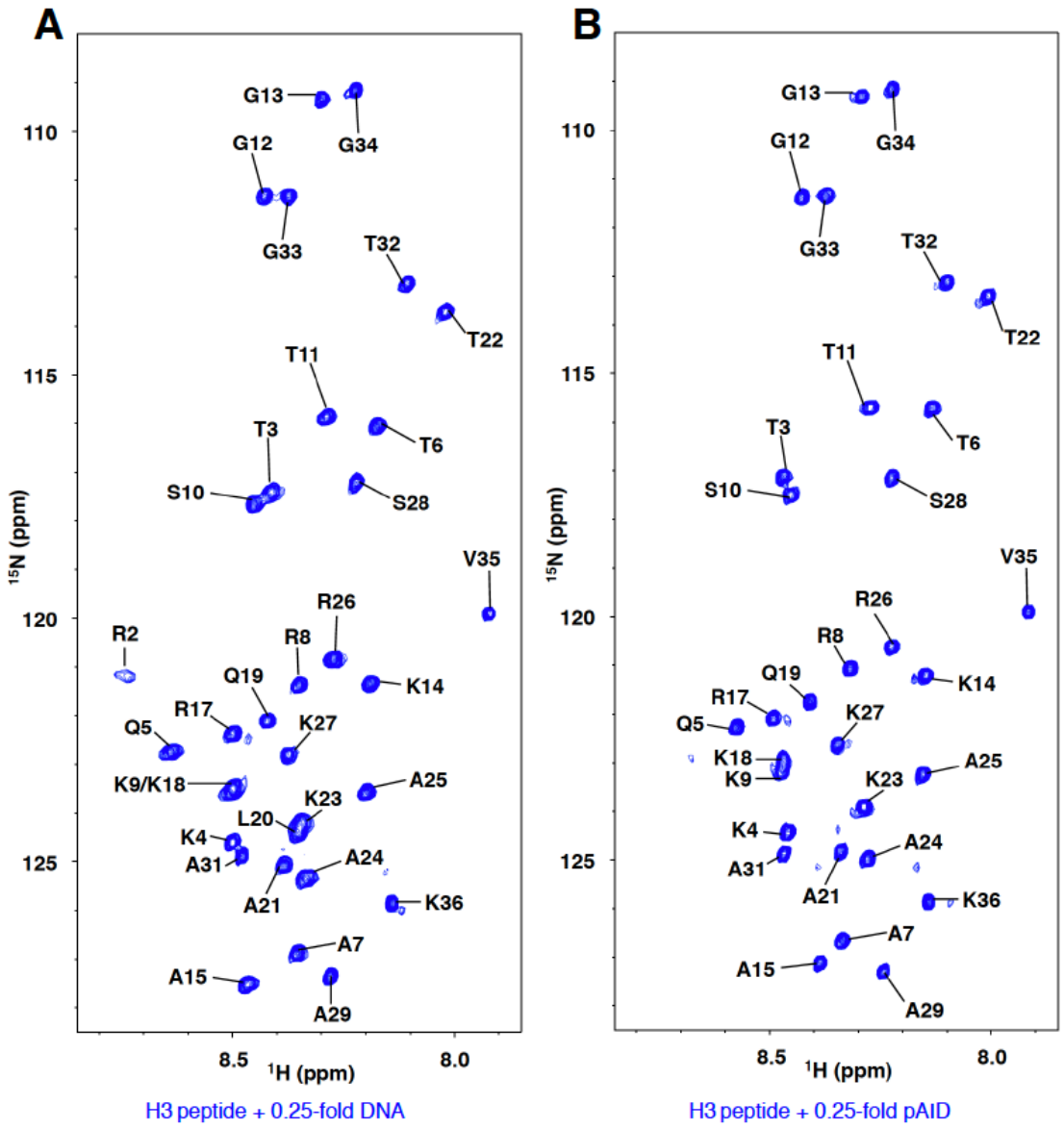

Figure S5. Related to Figure 6. NMR spectra of the H3 peptide upon the addition of DNA or pAID.

(**A**) 2D ^{1}H-^{15}N HSQC spectrum of the H3 peptide upon the addition of 33-bp DNA at a molar ratio of 1:0.25.

(**B**) 2D ^{1}H-^{15}N HSQC spectrum of the H3 peptide upon the addition of pAID at a molar ratio of 1:0.25.

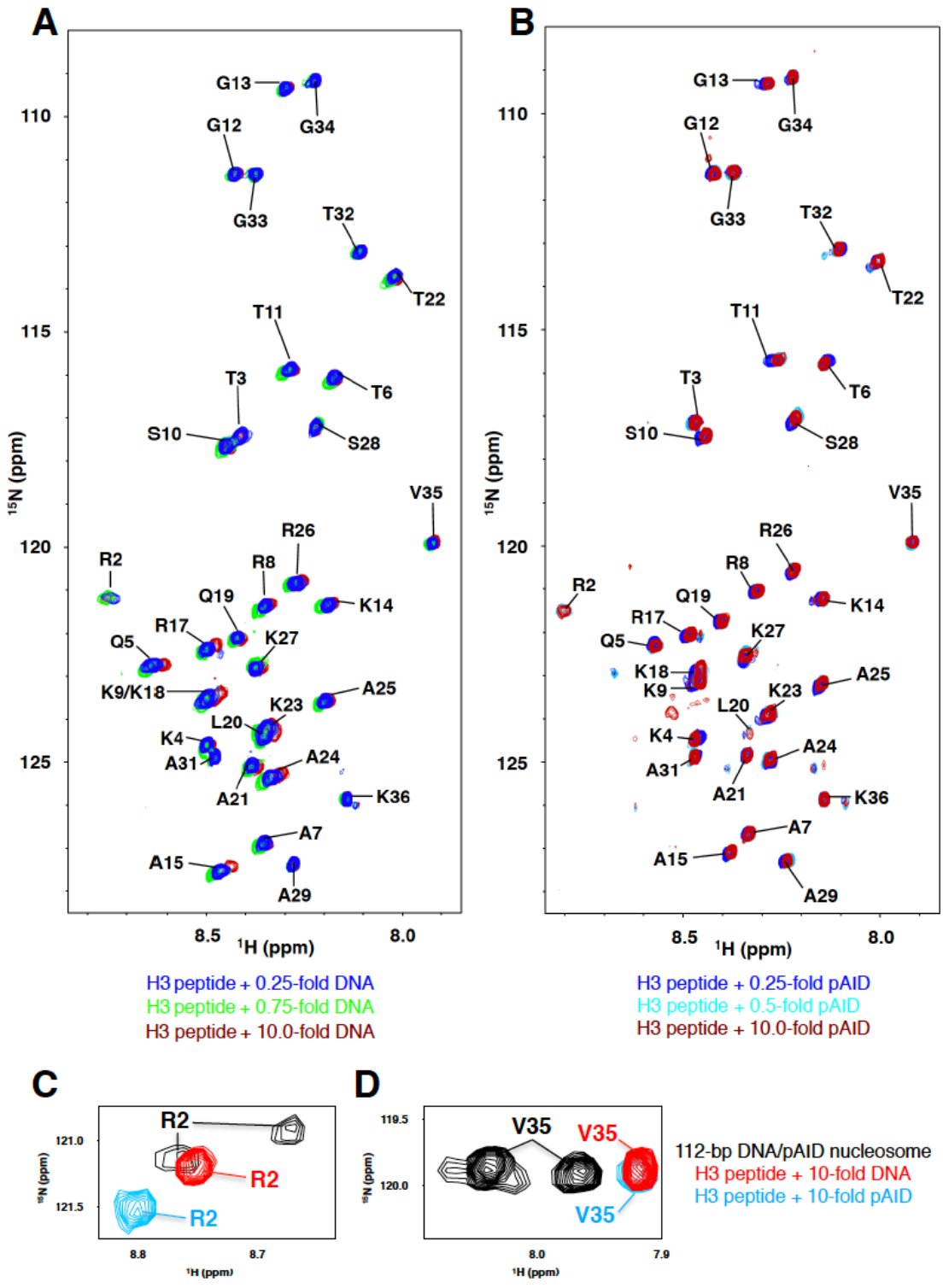

Figure S6. Related to Figure 6. NMR spectra of the H3 peptide upon the titration of DNA or pAID.

(**A**) Spectral superposition of the 2D ^{1}H-^{15}N HSQC spectra of the H3 peptide upon titration with 33-bp DNA at a molar ratio of 1:0.25 (blue), 1:0.75 (green),

and 1:10 (brown).

(**B**) Spectral superposition of the 2D ^{1}H-^{15}N HSQC spectra of the H3 peptide upon titration with pAID at a molar ratio of 1:0.25 (blue), 1:0.5 (cyan), and 1:10 (brown).

(**C, D**) Spectral comparison of 2D ^{1}H-^{15}N HSQC spectra at Arg2 (C) and Val35 (D) between the H3 peptide upon the 10-fold addition of DNA (red) or pAID (cyan) and the 112-bp DNA/pAID nucleosome (black).

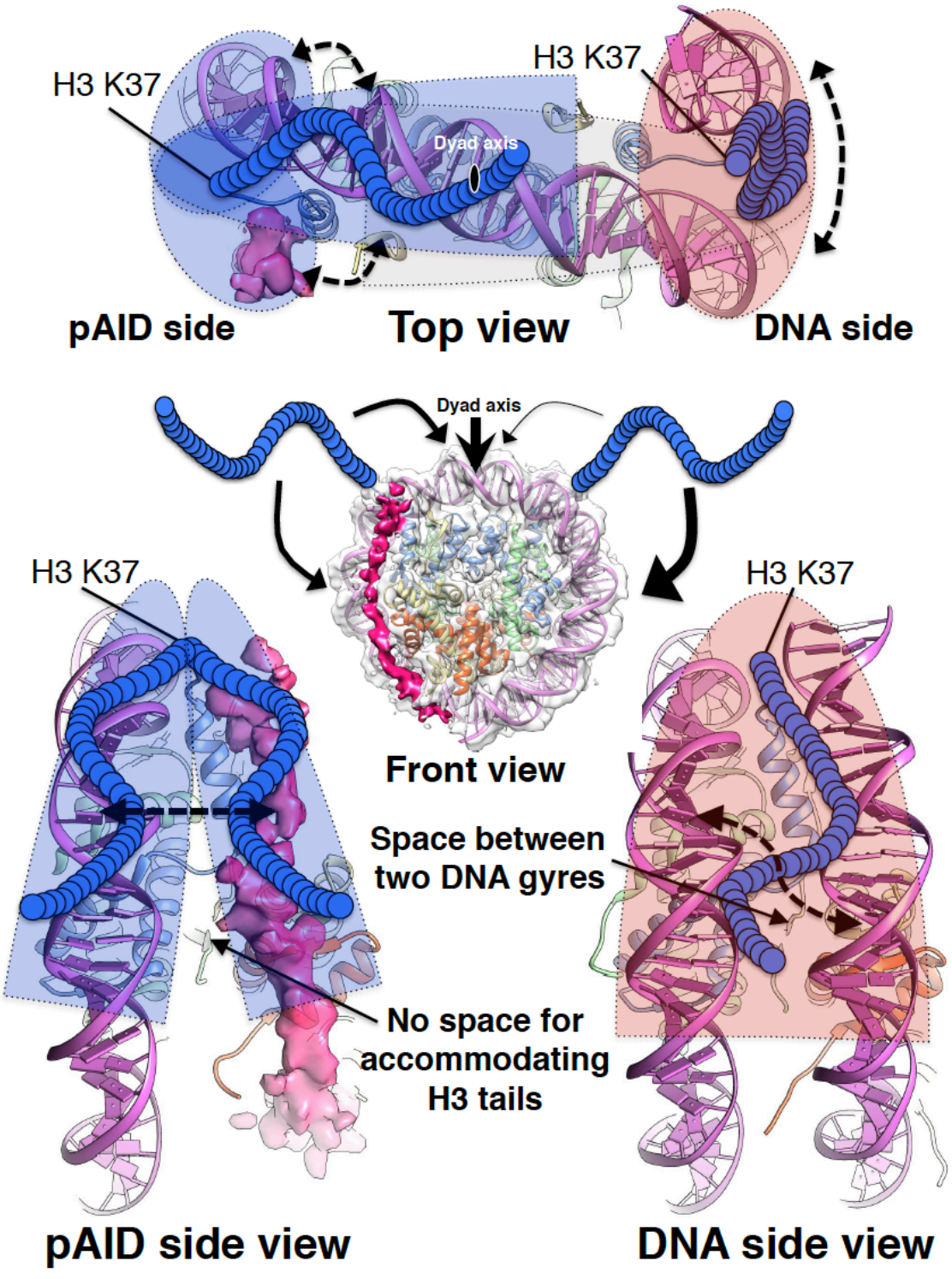

Figure S7. Related to Figure 7. Schematic views of the dynamic structure of the H3 N-tails at asymmetric locations in the 112-bp DNA/pAID nucleosome. Four different views of the EM density map (EMD-9639) superimposed on the nucleosome structure (PDB ID: 2CV5), colored as in Figure 1B, are shown. Blue

circular chains denote the H3 N-tails. The symbols indicating the dyad axis are based on the original nucleosome structure (top and front views). Black arrows represent the collapsed direction of the H3 N-tails (front view). Dotted arrows represent the dynamic behavior of the H3 N-tails (top and side views). The dashed ellipsoid, shaded in red and blue, represent the putative range of mobility of, respectively, the DNA and pAID side H3 N-tails in the 112-bp DNA/pAID nucleosome (top and side views).

Transparent Methods

RESOURCES TABLE

REAGENT or RESOURCE	SOURCE	IDENTIFIER
Bacterial and Virus Strains		
ECOS BL21(DE3) cells	NIPPON GENE	Cat# 314-06533
DH10Bac cells	Thermo Fisher	Cat#10361012
Chemicals, Peptides, and Recombinant Proteins		
Recombinant human histones	Tsunaka et al., 2005	N/A
Recombinant human FACT protein	Tsunaka et al., 2016	N/A
Recombinant human pAID protein	Mayanagi et al., 2019	N/A
Recombinant human H3 peptide	Ishiyama et al., 2017	N/A
Recombinant human Gcn5 catalytic domain	Enzo Life Sciences	Cat#BML-SE272-0050
HAT Assay Kit (Fluorescent)	Active-motif	Cat#56100
SYBR Gold Nucleic Acid Gel Stain	Thermo Fisher	Cat#S11494
Deposited Data		
Cryo-EM map of 112-bp octasome/pAID complex	Mayanagi et al., 2019	EMDB: 9639
The atomic nucleosome model determined by X-ray crystallography	Tsunaka et al., 2005	PDB: 2CV5
Experimental Models: Cell Lines		
Spodoptera frugiperda: Sf9 insect cells	Thermo Fisher	Cat#11496-015
Oligonucleotides		
33-mer 601_1 5′-ATCAGAATCCCGGTGCCGAGGCCGCTCAATTGG-3′	Thermo Fisher	N/A
33-mer 601_2 5′-CCAATTGAGCGGCCTCGGCACCGGGATTCTGAT-3′	Thermo Fisher	N/A
Recombinant DNA		
pET-H2A	Tsunaka et al., 2005	N/A
pET-H2B	Tsunaka et al., 2005	N/A
pET-H3.1	Tsunaka et al., 2005	N/A
pET-H4	Tsunaka et al., 2005	N/A

pFastBacDual-HisSPT16-SSRP1	Tsunaka et al., 2016	N/A
pColdI-pAID (residues 926-964)	Mayanagi et al., 2019	N/A
pGEX-ST1-histone H3 (residues 1-36+37W)	Ishiyama et al., 2017	N/A
pRSFduet-Casein Kinase 2	Mayanagi et al., 2019	N/A
Tvector-145-bp 601 DNA	Tsunaka et al., 2016	N/A
Tvector-112-bp 601 DNA	Tsunaka et al., 2016	N/A
Software and Algorithms		
UCSF Chimera	Pettersen et al., 2004	https://www.cgl.ucsf.edu/chimera/
NMRPipe	Delaglio et al., 1995	https://www.ibbr.umd.edu/nmrpipe/install.html
Gnuplot	http://gnuplot.info/	v5.0
Olivia v1.16.9	M. Yokochi, S. Sekiguchi & F. Inagaki, Hokkaido University, Sapporo, Japan	https://github.com/yokochi47/Olivia

Protein expression and purification

Recombinant human histone proteins were produced in *Escherichia coli* and purified as described previously (Tsunaka et al., 2005). $^{2}H/^{15}N$-labeled or $^{2}H/^{13}C/^{15}N$-labeled full-length histone H3 proteins and an H3 peptide, composed of the H3 N-tail residues Ala1–Lys36 and an additional Trp37 residue, were each expressed in 100% deuterated M9 minimal medium containing ^{15}N-ammonium chloride with or without ^{13}C-glucose. Baculovirus-driven expression of the human FACT (hFACT) complex (co-expression of N-terminal His-tagged SPT16 and non-tagged SSRP1) in Sf9 insect cells was carried out as reported previously (Tsunaka et al., 2016). The pAID protein, comprising human SPT16 residues 926–964, was expressed in *E. coli* strain BL21 (DE3) containing the expression plasmid pColdI (pAID) with pRSFduet (Casein Kinase 2) as reported previously (Mayanagi et al., 2019). The hFACT proteins were purified as described previously (Mayanagi et al., 2019; Tsunaka et al., 2016). All DNA segments are

based on the 601 nucleosome positioning sequence (Lowary and Widom, 1998). DNA fragments of 33-bp, 112-bp, and 145-bp were constructed and purified as described previously (Tsunaka et al., 2016). The 112-bp DNA/pAID nucleosome, 112-bp DNA/FACT nucleosome, and 145-bp nucleosome were reconstituted from histones, DNA fragments, and hFACT proteins by the salt dialysis method, and then purified as described previously (Mayanagi et al., 2019). The H3 peptide was purified according to previously published protocols (Ishiyama et al., 2017) with a few modifications. Cells were suspended in buffer containing 150 mM NaCl, 20 mM Tris-HCl, pH 7.6, and 1 mM DTT, and lysed by sonication. The GST-fused H3 peptide was partially purified on a GSTrap column (GE Healthcare) and the GST tag was removed by SUMO protease. The H3 peptide was applied to a HiTrap SP cation exchange column (GE Healthcare). Fractions containing the H3 peptide were further purified on a Superdex200 GF column (GE Healthcare).

NMR spectrometry

All NMR spectra were recorded at 293 K on 600-MHz and 950-MHz Bruker Avance III HD spectrometers, equipped with cryogenically triple-resonance pulsed-field gradient cryoprobes. All of them were processed with the program NMRPipe (Delaglio et al., 1995) and analyzed by the program Olivia (M. Yokochi, S. Sekiguchi & F. Inagaki, Hokkaido University, Sapporo, Japan). For backbone assignment, the 112-bp DNA/pAID nucleosome (80 μM) containing $^{2}H/^{13}C/^{15}N$-labeled histone H3 in NMR buffer (20 mM HEPES-NaOH pH 7.0, 10% D_2O) was used. Backbone resonances were assigned via the following experiments: TROSY-HNCACB, TROSY-HNCA, TROSY-HNCO, TROSY-HN(CA)CO and 2D TROSY-^{1}H-^{15}N HSQC. For other NMR experiments, reconstituted nucleosomal complexes (20–80 μM) containing $^{2}H/^{15}N$-labeled histone H3 and a $^{2}H/^{15}N$-labeled H3 peptide (30–100 μM) in NMR buffer were used.

Titration of 33-bp DNA or pAID into the $^{2}H/^{15}N$-labeled H3 peptide or the $^{2}H/^{15}N$-labeled 112-bp DNA/pAID nucleosome was performed in NMR buffer at 293 K. The change in signals caused by substrate titration were monitored by TROSY-^{1}H-^{15}N HSQC. Titration of NaCl into the 145-bp nucleosome containing

$^{2}H/^{15}N$-labeled histone H3, and addition of 20 mM Na/K phosphate buffer, pH 7.0, to the $^{2}H/^{15}N$-labeled H3 peptide were performed by the same method. Chemical shift differences (Δδ) were calculated according to $\Delta\delta = \{(\Delta\delta^{1}H)^{2} + (\Delta\delta^{15}N/5)^{2}\}^{1/2}$.

Heteronuclear NOE experiments

^{1}H-^{15}N heteronuclear NOE experiments were performed at 293 K on the ^{15}N-labeled 112-bp DNA/pAID nucleosome and the ^{15}N-labeled 145-bp nucleosome in the NMR buffer using a Bruker Avance III HD 600-MHz spectrometer and TROSY-type pulse sequence. Before measurements, ^{1}H signals were saturated by applying successive irradiation of 120-degree pulses at 5-ms intervals for 5 seconds, and the intensities of the irradiated signals were compared with those of the un-irradiated signals.

NMR real-time monitoring of acetylation reaction

Acetylation reactions of the 112-bp DNA/pAID nucleosome, the 145-bp nucleosome, and the H3 peptide upon 0.25-fold addition of 33-bp DNA (1.6–2.5 nmol of each substrate) were carried out in NMR buffer using 0.2 nmol of human Gcn5 catalytic domain (Enzo Life Sciences) in presence of 360 nmol of Acetyl-CoA at 0 or 200 mM NaCl. Enzymatic reactions were continuously run for 64 hours at 293 K. Spectra were measured every hour.

Electrophoretic mobility shift assays (EMSAs)

The 145-bp nucleosome (1.5 pmol) was mixed with pAID or hFACT proteins (each 1.5 pmol) in 20mM Tris-HCl, pH 7.0. These samples, the 145-bp nucleosome, the 112-bp DNA/pAID nucleosome, and the 112-bp DNA/FACT nucleosome (each 1.5 pmol) were incubated for 15 min at 30 °C in a reaction buffer containing 150 mM NaCl, 20 mM Tris-HCl, pH 7.6. The samples were separated by electrophoresis at 4 °C on a 7.5% native-PAGE in 1 × Tris-glycine buffer, and were visualized by SYBR Gold nucleic acid gel stain.

Fluorescence HAT assay

HAT reactions were performed for 17 hours at 25 °C using 20 pmol of nucleosomes, hFACT proteins, and the mixed samples in the presence of 2 pmol of human Gcn5 catalytic domain (Enzo Life Sciences) and 2.5 nmol of Acetyl-CoA in 20 mM Tris-HCl pH 7.0 in a total volume of 50 µl. The HAT reaction was quantified by the detection of CoA-SH after the reaction using the Fluorescent HAT Assay Kit (Active-motif). The reported values have been subtracted for the intensity of samples in which substrates were added to the mixtures after the reaction. Fluorescence intensities were detected by using Varioskan Flash 2.4 (Thermo Scientific). All data were normalized to the mean intensities of at least three independent reactions.

Quantification and statistical analysis

Quantification and statistical details of experiments can be found in the relevant figure legends.

Supplemental References

Delaglio, F., Grzesiek, S., Vuister, G., Zhu, G., Pfeifer, J., Bax, A., 1995. NMRPipe: a multidimensional spectral processing system based on UNIX pipes. J Biomol NMR 6, 277–293.

Ishiyama, S., Nishiyama, A., Saeki, Y., Moritsugu, K., Morimoto, D., Yamaguchi, L., Arai, N., Matsumura, R., Kawakami, T., Mishima, Y., Hojo, H., Shimamura, S., Ishikawa, F., Tajima, S., Tanaka, K., Ariyoshi, M., Shirakawa, M., Ikeguchi, M., Kidera, A., Suetake, I., Arita, K., Nakanishi, M., 2017. Structure of the Dnmt1 Reader Module Complexed with a Unique Two-Mono-Ubiquitin Mark on Histone H3 Reveals the Basis for DNA Methylation Maintenance. Mol. Cell 68, 350–360.

Lowary, P.T., Widom, J., 1998. New DNA sequence rules for high affinity binding to histone octamer and sequence-directed nucleosome positioning. J Mol Biol 276, 19–42.

Mayanagi, K., Saikusa, K., Miyazaki, N., Akashi, S., Iwasaki, K., Nishimura, Y., Morikawa, K., Tsunaka, Y., 2019. Structural visualization of key steps in nucleosome reorganization by human FACT. Sci Rep 9, 10183.

Pettersen, E.F., Goddard, T.D., Huang, C.C., Couch, G.S., Greenblatt, D.M., Meng, E.C., Ferrin, T.E., 2004. UCSF Chimera - a visualization system for exploratory research and analysis. J. Comput. Chem. 25, 1605–1612.

Tsunaka, Y., Fujiwara, Y., Oyama, T., Hirose, S., Morikawa, K., 2016. Integrated molecular mechanism directing nucleosome reorganization by human FACT. Genes Dev. 30, 673–686.

Tsunaka, Y., Kajimura, N., Tate, S., Morikawa, K., 2005. Alteration of the nucleosomal DNA path in the crystal structure of a human nucleosome core particle. Nucleic Acids Res 33, 3424–3434.